BIo-Inspired Fluid Locomotion

by

Brian Chan

Submitted to the Department of Mechanical Engineering
in partial fulfillment of the requirements for the degree of

Doctor of Science in Mechanical Engineering

at the

MASSACHUSETTS INSTITUTE OF TECHNOLOGY

August 20XX

Author .....
Department of Mechanical Engineering
May 1, 20XX

Certified by .....
Anette Hosoi
Associate Professor
Thesis Supervisor

Accepted by .....
David Hardt
Head, Department of Mechanical Engineering

BIo-Inspired Fluid Locomotion

by

Brian Chan

Submitted to the Department of Mechanical Engineering
on May 1, 20XX, in partial fulfillment of the
requirements for the degree of
Doctor of Science in Mechanical Engineering

Abstract

We have developed several novel ways of locomotion at low Reynolds number, for Newtonian and non-Newtonian fluids: Robosnail 1 and 2, which operate on a lubrication layer, and the three-link swimmer which moves in the free fluid. Robosnail 1 utilizes lubrication pressures generated in a Newtonian fluid under a steadily undulating foot to propel itself forward. Tractoring force and velocity measurements show reasonable agreement to analytic and numerical solutions. Robosnail 2, modeled after real land snails, uses in-plane compressions of a flat foot on a mucus substitute such as Laponite or Carbopol. Robosnail 2 exploits the non-Newtonian qualities (yield-stress, shear thinning) of the fluid solution to locomote. The glue-like behavior of the unyielded fluid allows Robosnail 2 to climb up a 90 degree incline or inverted 180 degree surfaces. The three-link swimmer is a device composed of three rigid links interconnected by two out-of-phase oscillating joints. It is the first experimental test that successfully proves that a swimmer of its kind can swim forward in the Stokes limit.

Thesis Supervisor: Anette Hosoi
Title: Associate Professor

Acknowledgments

The Author would like to thank David Hu and John Bush for their assistance.

Contents

List of Figures

List of Tables

Chapter 1

Introduction

The realm of the low-Reynolds number encompasses the world of the very small, the very viscous, or the very slow. If we were to shrink the size of a microbe, or to swim in a pool of honey, or to slow our motions to a snail's pace, we would catch a glimpse of this world. It would appear to us very alien because of the different physical laws that dominate. At this scale, the simple task of getting around involves strategies that are often counterintuitive and not applicable to the larger scales in which we live. Fortunately for us, it is not difficult to study this world, since varying the Reynolds number only requires changing the speed, length, or fluid viscosity, and not necessarily all three together. This way, we can understand microscopic systems by building a macroscale experiment and controlling the speed and/or fluid viscosity to achieve the correct Reynolds number.

Observations of low Re organism suggests that the realm of low Re required a very different type of locomotion. Most such swimmers do not resemble the macroscale (high Re) swimming and flying organisms we are used to seeing. Instead of wings, fins, and flaps, we find mostly cilia and flagella as the dominant means of propulsion. One of the first researchers of low-Re locomotion was G. I. Taylor [7], who introduced the idea of reversible flow at low Re. Taylor also looked into the mechanics of flagellar propulsion, and built simple flagellar swimmers to demonstrate their efficacy. Another low-Re device, proposed by E.M. Purcell [6], was the three-link swimmer, hypothetically the simplest mechanism of oscillating links capable of locomotion in the Stokes limit (Re = 0). While Purcell had proposed that such a swimmer should be able to generate a displacement, no real prototype of this mechanism has been made until now.

While the locomotion of small mobile objects in the free fluid at low Re has been well studied, the motion of organisms over a thin layer of fluid has been covered relatively little. Vlès [8] made one of the first detailed observations in writing of the contractile motions of the snail's foot during locomotion. Decades later, Lissman [5, **?**] made detailed kinematic observations of the foot motions of snails and hypothesized certain ways that a snail might use a single foot to move over different surfaces. Denny [3, 4, 2], was the first to recognize that the non-newtonian properties of snail mucus played an important role in locomotion.

The research in snail locomotion has inspired a branch of low-Reynolds number locomotion based on peristaltic waves. It has been known that motions of boundaries over thin layers of viscous fluid can generate very large shear and normal stresses in the low - Re lubrication regime. While engineers have long taken advantage of these lubrication forces in the design of bearings, we sought to prove that similarly forces could be used for propulsion. To the best of our knowledge, until Robosnail 1, there has been no prior experimentation

with free self-propelled peristaltic movers over thin fluids.

1.1 Motivations for Low-Re Locomotion

There are numerous emerging technologies that will make use of low-Re flows and low-Re locomotion. Microfluidic devices, commonly known as "lab-on-a-chip" devices, will be able to perform numerous fluid experiments (such as a blood test) using only a fraction of a sample droplet. Our understanding of low-Re flow will help us manipulate flows in such devices. Miniature swimming machines may soon be used to navigate tiny fluid-filled passageways of the human body. As manufacturing methods become increasingly capable of creating and assembling micro-scale components, these miniature swimmers will become more widespread. A good general theory of low-Re locomotion will be necessary to design these miniature swimming devices.

1.2 Motivations for Snail-Inspired Locomotion

The majority of this research has its focus in snail-inspired locomotion. Snails possess a mode of locomotion that is radically different from that of most other organisms, with the possible exception of worms. The simplicity of the foot structure (a single muscular foot) suggests that we should be able to design simple machines likewise capable of a variety of useful motions. When artificial muscle-like actuators become more widespread, they could conceivably be joined together easily to make simple snail-like actuators. Snail-like locomotion devices should be effective anywhere provided there are viscous fluids. If the fluids are non-Newtonian, there can be further advantages, such as the ability to climb walls, which was one of the design goals of Robosnail 2.

In addition to micro-robotics, the field of oil drilling could potentially benefit greatly from the application of snail-like devices. The setting of an oil well can be highly challenging as they are often muddy, vertical and irregular. A flexible slug-like or snail-like device may be more adept at navigating the messy environment of a downhole than a more conventional rigid, jointed mechanism.

1.3 Description of snail locomotion

What snails lack in speed, they make up for in versatility. Snails are capable of climbing walls and ceilings, as well as traversing some very rough, irregular terrains, and are not hindered by wet surfaces. They accomplish this by carrying their own fluid lubrication, mucus. As the snail moves its muscular foot, the forces are transmitted to the substrate through the thin mucus layer. Thus the study of snail locomotion is a study of fluid dynamics. The viscous, non-Newtonian mucus and complex motions of the foot seem to be optimized for the snail's unique way of locomotion.

The most important property of mucus that allows a snail to exhibit such versatility in locomotion is its finite yield stress. In other words, the mucus, even though it is more than 90% water, behaves as a solid unless it is stressed past a certain amount. The ability of the mucus to solidify allows a snail to maintain traction on a variety of surfaces, to climb walls, and to remain stuck on a wall or ceiling even when it is not moving.

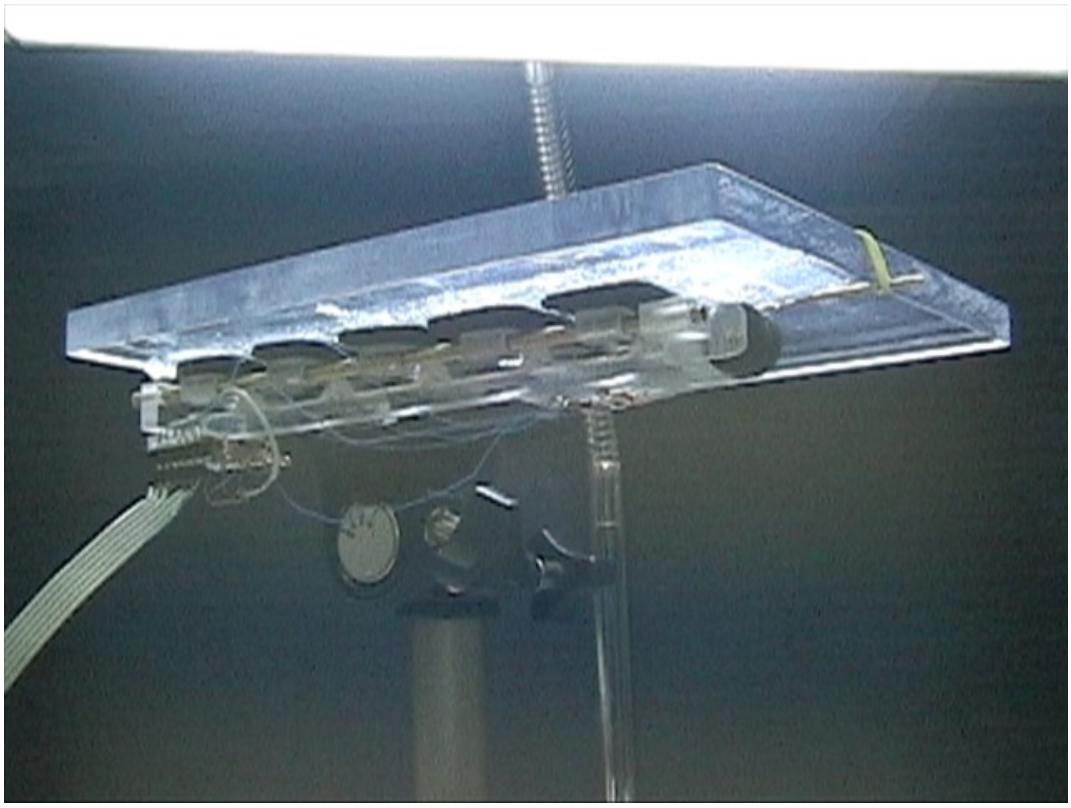

Figure 1-1: One prototype of robosnail 2, moving in an inverted position

1.4 Description of various Robosnails

We have constructed two types of the mechanical snail, Robosnail 1 which uses a waving foot to move over viscous newtonian fluids, and Robosnail 2 that uses a sliding foot to move over a shear-thinning fluid. The physical models of each locomotion method are distinctly different from one another. In terms of biomimicry, Robosnail 2 is the closest to the functioning of real snails, using adhesion and sliding rather than peristalsis and lubrication pressures as in the case of Robosnail 1. While Robosnail 2 is constrained by the limitation that it requires non-newtonian fluid to operate, it is capable of such feats as moving up walls or in an inverted position. Both types of snail were explored in some depth, and the results are presented here.

1.5 Description of three-link swimmer

The three link swimmer, like the robosnails, is the first machine of its type to be constructed. It is theoretically one of the simplest machines that theory predicts is able to swim in the stokes limit. Physically, it can be thought of as a free-swimming cousin to the peristaltic waving robosnail, where the waving motion is discretized into three rigid sections rather than a continuous, smooth wave. However, the three link swimmer has given rise to further research into n-link swimmers which approach the continuous limit. Because of the complex nature of the flow around the three-link swimmer, few equations are presented; however, the experimental results increase our understanding of the swimmer's behavior at low Reynolds

number.

These devices together represent a diverse range of approaches to locomotion in viscous fluids, and have sparked a new generation of propulsive devices for locomotion at low Reynolds numbers.

Chapter 2

General Theory

2.1 Locomotion at Low Reynolds Number

All of the systems described here operate at extremely low Reynolds number, the regime where viscous forces dominate over all inertial and buoyant forces. In this limit, the Navier-Stokes equations reduce to the Stokes equations. The Navier-Stokes equations for incompressible Newtonian fluids,

$$\nabla \cdot v = 0$$

$$\rho(\frac{\partial v}{\partial t} + v \cdot \nabla v) = -\nabla p + \mu \nabla^2 v + f \tag{2.1}$$

where ρ is the fluid density, v is the velocity field, p is the pressure, μ is the fluid viscosity, and f is an applied body force on the fluid.

The Reynolds number describes the relative magnitudes of inertial and viscous forces:

$$Re = \frac{\rho V L}{\mu}$$

Where V and L are characteristic velocities and lengths in the flow. In the absence of body forces, at the limit of low Reynolds number (usually when V or L, the right-hand terms Navier-Stokes equation become zero and $f = 0$, resulting in the Stokes equation:

$$\nabla \cdot v = 0$$

$$\nabla p = \mu \nabla^2 v \tag{2.2}$$

2.2 Lubrication Flows

When the fluid in question is constrained to flow inside a thin fluid gap, further simplifications can be made to the analysis and the Navier-Stokes equations involved. In this limit, the Stokes equations reduce even further to the lubrication equation:

$$\frac{\partial p}{\partial x} = \frac{\mu \partial^2 u}{\partial y^2}$$

The pressure of the fluid varies only along the direction of the film, momentum effects are negligible.

2.3 Snail Locomotion

A generalized snail of this type should have a continuous foot, with a thin mucus layer of variable height, whose surface moves with an predefined cyclic motion. Thus, while the foot is flexible and each point on the foot moves independently, the average velocity of any one point on the foot is equal to the average velocity of the snail itself.

The net force on the snail from the fluid is the integral of all the fluid forces acting on the foot. At the low Reynolds numbers involved, all flows can be considered quasi-steady, so acceleration terms are ignored:

$$F_t = \int_A dF = \int_A \tau dA + \int_A p dA$$

where F_t is the tractoring force (the force required to pull a given payload, or any given external force), A is the total area of the foot, τ is the shear stress in the fluid tangential to the foot surface, and p is the pressure within the fluid. Theoretically, a snail can generate propulsive forces from any combination of pressure and shear forces. In our case, we separate the test the two phenomenon separately. Robosnail 1 is a pressure-driven mechanism, while Robosnail 2 relies on shear forces.

2.3.1 Shear-thinning fluids

While Newtonian fluids have a constant viscosity and therefore a linear response to increasing strain rate, non-newtonian fluids have variable viscosity and a non-linear response. There exist numerous different types of non-newtonian fluids, such as shear thickening fluids, shear thinning fluids, etc. Snail mucus is a shear thinning fluid with some viscoelasticity. The most important property that allows snails to move is the shear-thinning behavior.

In its most basic definition, a shear-thinning fluid is one which has a viscosity that decreases with increasing shear rate. The following plot shows the shear rate - viscosity relationship of Carbopol, the main fluid used to test Robosnail 2. Carbopol is a synthetic thixotropic fluid, chosen for its rheological similarity to real snail mucus.

Two secondary properties that affect snail locomotion are the finite yield stress and the restructuring time. Carbopol and snail mucus, for our purposes, can be classified as types of finite yield stress fluid, which is one particular type of shear-thinning fluid. The finite yield stress fluids, as opposed to general shear-thinning fluids, allow the snail to move upside-down on surfaces, and to passively glue themselves to vertical or inverted surfaces when they are not moving. This is possible because the fluid has a range of possible stresses under which the fluid effectively remains solid, gluing certain parts of the snail onto the substrate.

To be more accurate, snail mucus does not have a true solid state, but a high viscosity (in the "unyielded" regime) where the viscosity is many orders of magnitude higher than in the "yielded" regime. The high viscosity is so great and the resultant flow rates are so low that the fluid can be practically considered a solid.

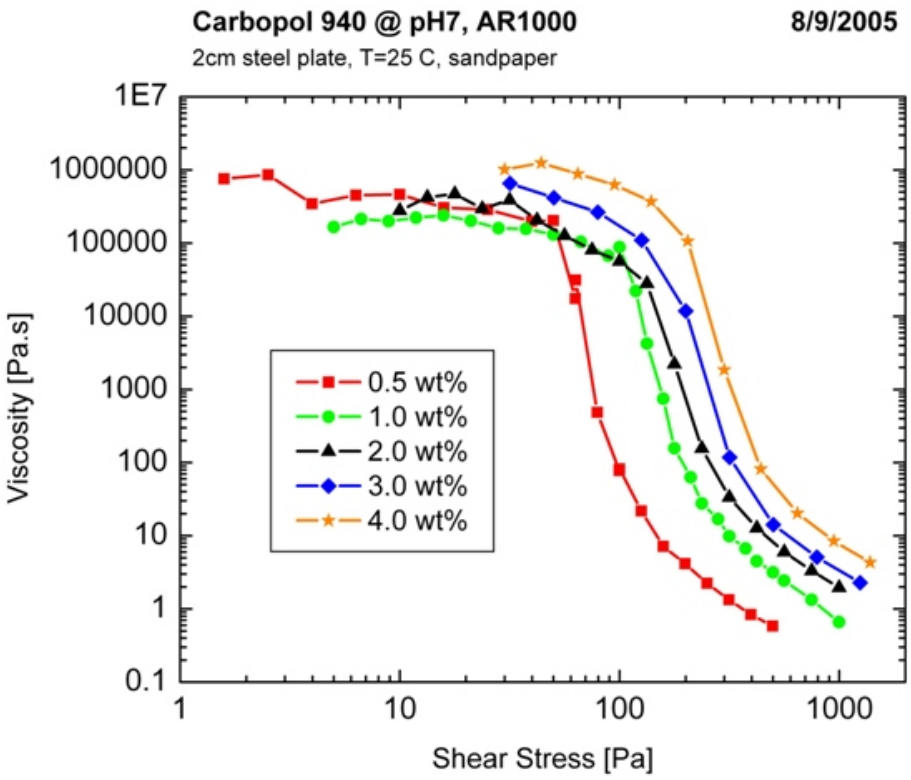

Figure 2-1: Shear-rate / viscosity curves for various concentrations of Carbopol, a synthetic fluid used for the lubrication layer of Robosnail 2. Note that for each curve, the viscosity begins to drop several orders of magnitude after a certain shear rate. This is the shear-thinning behavior; Newtonian fluids would have a constant viscosity regardless of shear rate. The shear-thinning property is a critical property that allows Robosnail and most snails to move.

Chapter 3

Robosnail 1

3.1 Introduction

Many organisms use undulation as a means to move through fluids, or to transport fluids. Robosnail 1 was built with the intention to emulate peristaltic crawlers, using a flexible, powered foot to move over a layer of viscous newtonian fluids, but as we shall see in the following chapter, this type of crawling is more "snail-inspired" than "snail-like." In actuality most snails use a different mode of locomotion (which we explored with the Robosnail 2 prototypes), but we decided to continue pursuing the undulating snail model. Regardless of its abundance in nature, peristaltic lubrication propulsion has proven to be an effective mode of transportation.

The basic idea of robosnail 1 is to use a waving sheet to squeeze viscous fluids backwards through the thin gap between snail and substrate. The reaction force of the fluid on the snail propels the snail forwards. Our initial concept machines could undulate a thin rubber foot over a layer of glycerol, and thus propel themselves at a speed close to the undulation speed.

3.2 Theory

3.2.1 Underlying physics

Robosnail 1 locomotion is analogous to peristaltic pumping, for example the movement of fluid through the intestine is due to the peristaltic motion of the intestinal wall. In Robosnail 1, the foot is like the pumping wall, and as with peristaltic pumping, the wall exerts a force on the fluid. Unlike peristaltic pumping, the fluid in turn transmits the force on the substrate which causes motion of the pumping device. The changing shape of the snail foot is described by the fluid thickness height $\hat{h}(x,t)$, which varies with time. For simplification of analysis, we assume that the waving membrane is periodic with a wavelength λ such that $\hat{h}(x,t) = \hat{h}(\hat{x} + n\lambda, t)$ and that the waves travel with a speed $\hat{V}_w$ such that $\hat{h} = f(\hat{x} - \hat{V}_w t)$. We define the average height $\hat{H} = av(\hat{h})$ and an amplitude $\hat{a} = \hat{H} - min(\hat{h})$The snail travels at some resultant velocity $\hat{V}_s$. For practical concerns, it may also be tugging some payload (or tractoring force) $\hat{F}_t$.

Natural mucus used by snails is a viscous, non-newtonian fluid which has a variable viscosity dependent on shear rate. As shown in later chapters, real snails exploit these non-newtonian properties in their method of locomotion; their motions would be severely

handicapped if their mucus were a newtonian fluid. Because robosnail 1 relies on newtonian effects, the 'mucus' used with robosnail 1, can be a viscous newtonian fluid, and will be modeled as such. Since the layer of fluid is thin, we assume that the lubrication approximation holds everywhere in the fluid film. Under this assumption, pressure varies in the $x-$ and $y-$ directions, but not in the $z-$ axis. Also, because inertial effects are much smaller than viscous effects, the flow is considered quasi-steady. In this limit, the Navier-stokes equations reduce to:

$$\mu \frac{\partial^2 u}{\partial z^2} = \frac{\partial \hat{p}}{\partial \hat{x}}$$

At this point it becomes useful to non-dimensionalize the equations, rescaling the relevant quantities as follows:

$$\hat{x} = \lambda x$$

$$\hat{z} = \hat{H} z$$

$$\hat{u} = \hat{V_w} u$$

$$\hat{p} = \frac{\lambda \mu \hat{V_w}}{\hat{H}^2} p$$

$$\hat{h} = \hat{H} h$$

$$\hat{V_s} = \hat{V_w} V_s$$

and

$$\hat{F_t} = \frac{\lambda^2 \mu \hat{V_w}}{\hat{H}^2} f_t$$

The lubrication equation becomes:

$$\frac{\partial^2 \hat{u}}{\partial z^2} = \frac{\partial p}{\partial x}$$

in dimensionless form.

For thin profiles, pressure does not vary across the depth of the film. Hence, for any given x-position, the pressure is constant. The flow profile then must be parabolic for any given x-position, taking the form

$$\frac{du}{dz} = \frac{\partial p}{\partial x} z + C_1$$

$$u(z) = \frac{\partial p}{\partial x} z^2 + C_1 z + C_2 \tag{3.1}$$

where the integration constants C_1 and C_2 are determined by boundary conditions at the foot and the substrate. To solve for these constants we switch to a reference frame traveling with the wave. In this frame, the height function of the foot $h(x)$ does not vary with time. Because the flow is steady, the volume flow rate $Q = \int u dz$ (per unit width) is a constant. The top and bottom surface velocities in the new reference frame are:

$$\hat{V}|_{z=0} = \hat{V_w} - \hat{V_s}$$

$$\hat{V}|_{z=h} = \hat{V_w}$$

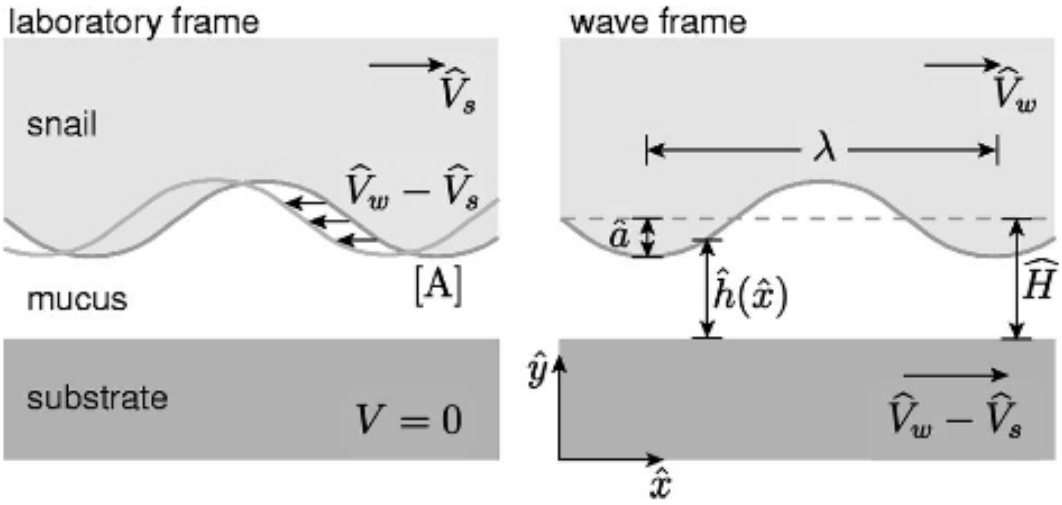

Figure 3-1: Switching to a useful reference frame for solving the flow underneath a self-propelled, peristaltic waving membrane. In the laboratory frame, the foot height is a function of x and t . In the wave frame (a frame of reference following the wave crests) the height is only dependent on x and the flow can be modeled as steady.

or in dimensionless terms,

$$u|_{z=0} = 1 - V_s$$

$$u|_{z=1} = 1$$

Applying these boundary conditions to equation 3.1, the velocity profile becomes

$$u(z) = \frac{1}{2}\frac{\partial p}{\partial x} z(z-h) + V_s(\frac{z}{h} - 1) + 1 \tag{3.2}$$

We can solve for Q by integrating $Q = \int_0^h u dz$

$$Q = \frac{h^3}{12}\frac{dp}{dx} - h(1 - \frac{v_s}{2}) \tag{3.3}$$

solving for $\frac{dp}{dx}$,

$$\frac{dp}{dx} = \frac{12}{h^3}[h(1 - \frac{v_s}{2}) - Q] \tag{3.4}$$

Applying the periodic boundary condition

$$\int_0^1 \frac{dp}{dx} dx = p(1) - p(0) = 0$$

, integrating 3.4 and solving for Q gives

$$Q = (1 - V_s/2)\frac{I_2}{I_3} \tag{3.5}$$

where

$$I_j = \int_0^1 \frac{dx}{h^j}$$

Forces come from the viscous shear at the surface of the membrane, and from the high pressure zones where the foot is nearly touching the ground. The shear forces act parallel to the foot surface, and the pressure force acts perpendicular to it. We are mainly concerned with forces in the x- direction (vertical forces depend on the average pressure under the foot, which can vary arbitrarily according to initial conditions).

$$f_{shear,x} = \frac{du}{dz}|_{y=h} dA$$

$$f_{pressure,x} = \int_0^1 p \frac{dh}{dx}$$

$$f = f_{pressure,x} + f_{shear,x} = \int_0^1 \left(p\frac{dh}{dx} + \frac{du}{dz}|_{y=h} \right) dx$$

Integrating the pressure term by parts and substituting 3.4 for $\frac{dp}{dx}$ yields

$$f_{pressure,x} = \int_0^1 p\frac{dh}{dx}dx = \left(12I_1 - \frac{I_2^2}{I_3}\right)\left(1 - \frac{V_s}{2}\right) \tag{3.6}$$

$$3QI_2 = (3 - 2V_s)I_1$$

Substituting Q from equation 3.5 gives the relation between velocity and tractoring force of the snail:

$$V_s = \frac{6(1-A)}{4-3A} - \frac{f}{I_1(4-3A)} \tag{3.7}$$

Where the shape function

$$A = \frac{I_2^2}{I_1 I_3}$$

The relation between force and velocity takes the simple linear form of $f = f_{stall} - mV_s$ where f_{stall} is the stall force, and m is a constant. Their respective values can be found by rearranging terms in equation 3.7:

$$f_{stall} = 6I_1(1-A) \tag{3.8}$$

$$m = -I_1(4-3A)$$

When $V_s = 0$ the force reaches the stall force. As the applied force on the snail is decreased, the velocity increases linearly until it reaches the free velocity, $V_{s,free}$

$$V_{s,free} = \frac{6(1-A)}{4-3A} \tag{3.9}$$

Figure 3.7 illustrates this straightforward relationship, which can be used to predict the snail's resultant velocity given any applied force.

The free velocity and dimensionless stall force, which we will also call the stall-force constant, f_{stall}, is purely a function of the foot shape, because the I_j and A are functions

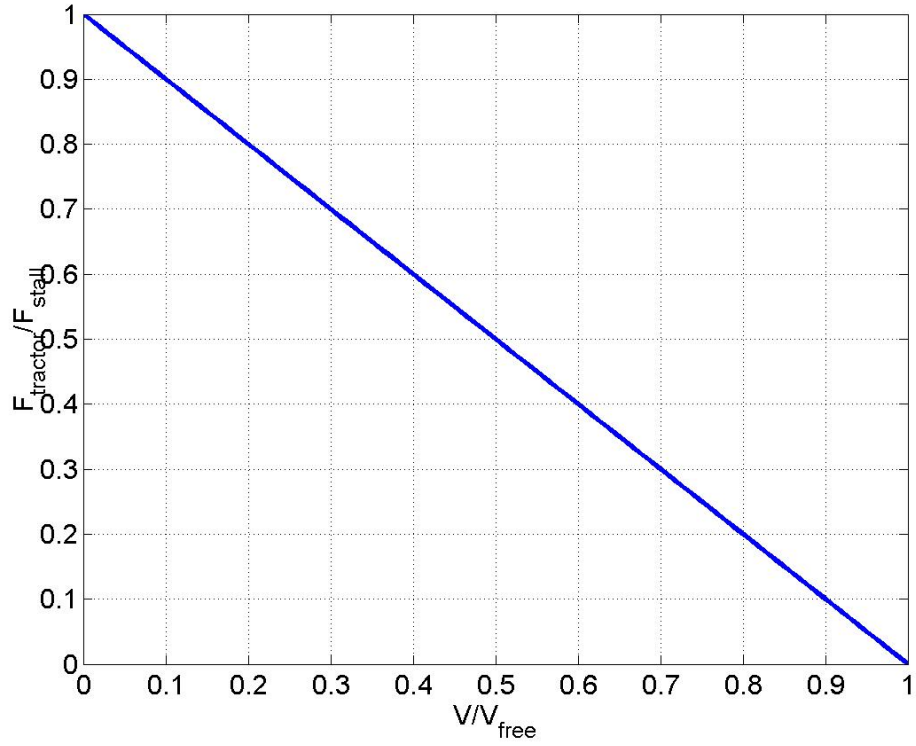

Figure 3-2: The relationship between dimensionless applied force and snail velocity. As the tractoring load is increased to the stall force, the velocity decreases to zero. The full graph extends past $f < 0$, where increasing the tractoring force beyond the stall force would cause the snail to drift backwards, and $V_s > V_{s,free}$ where a negative (pushing) tractoring force would increase the snail velocity past $V_{s,free}$.

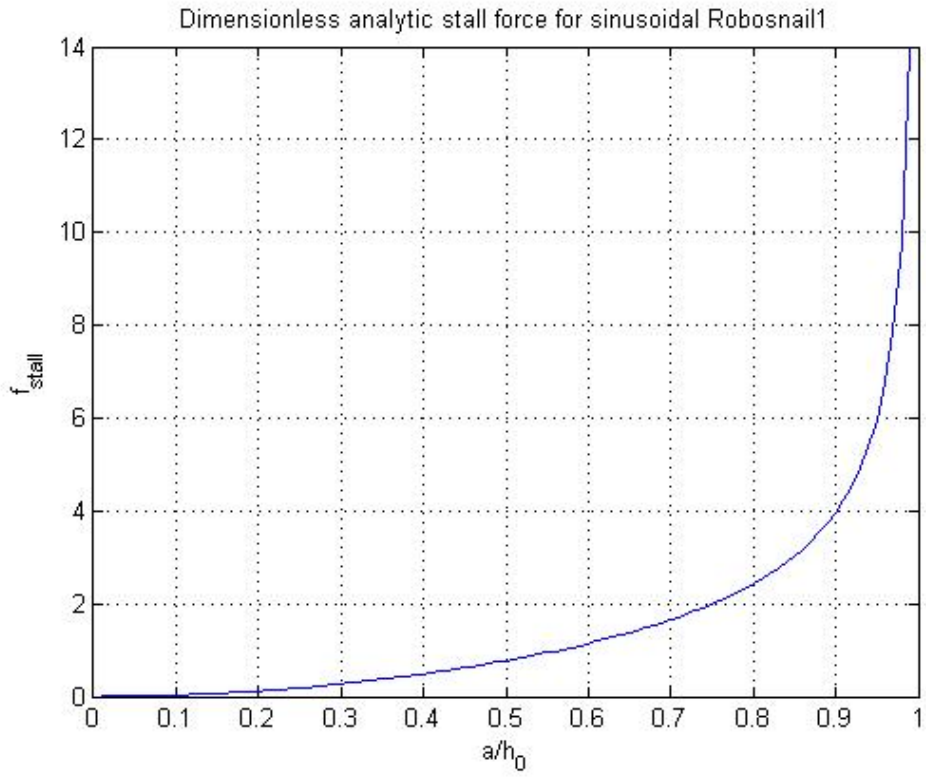

Figure 3-3: Dimensionless stall force for a sinusoidal waving foot. Note that as the amplitude gets larger, nearly touching down on the substrate, lubrication pressures increase, and the stall force increases greatly.

of the foot shape and of nothing else. For a sinusoidal foot, the foot shape is determined by a single dimensionless parameter, $\frac{a}{h_0}$ or the ratio of amplitude to average height. This is a practical parameter that states how close the foot is touching down to the ground, and is limited by $0 < \frac{a}{h_0} < 1$, that is to say, for any wave profile, it can be completely flattened setting $a = 0$, or touching the substrate when $a = 1$. In most engineering applications, one would want to maximize the stall force of a robosnail. The simplest way to increase the stall force is revealed by equation 3.2.1- by decreasing the clearance between the foot and the ground; other methods would be to increase the number of waves created by the foot, or to increase the viscosity of the working fluid, all of which are proportionally related to the dimensional stall force.

A practical result of the exact solution for a sinusoid is that the dimensionless waving velocity can be well-approximated by a linear relationship with coefficient 1, that is $v_s/v_w \; a/h_0$ This approximation is helpful for making predictions on the free velocity without having to redo the equations or run simulations.

An interesting note is that the resultant dimensionless force and velocity are merely a function of the wave shape. This is the same as for Stokes flow of self-propelled objects in an infinite fluid, the objects' motion is only a result of the geometry. For the snail, the problem is even more simplified, as the velocity and force can be predicted as long as the height is an integrable function.

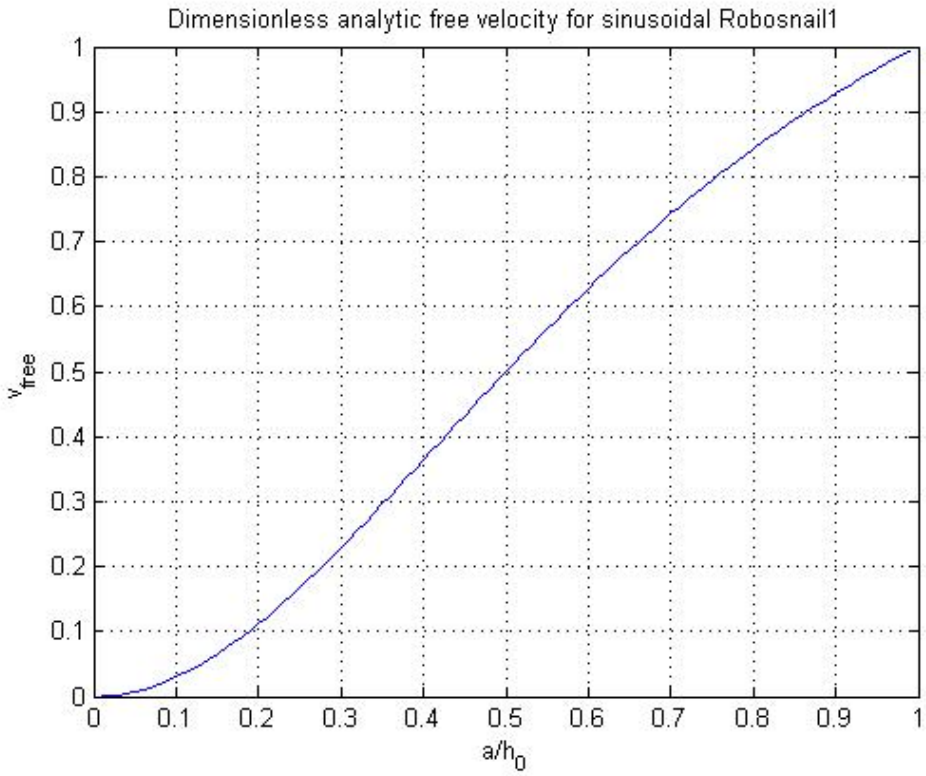

Figure 3-4: Theoretical dimensionless free velocity for a sinusoidal waving foot. Note that as the amplitude gets larger, nearly touching down on the substrate, the velocity of the snail approaches the waving velocity.

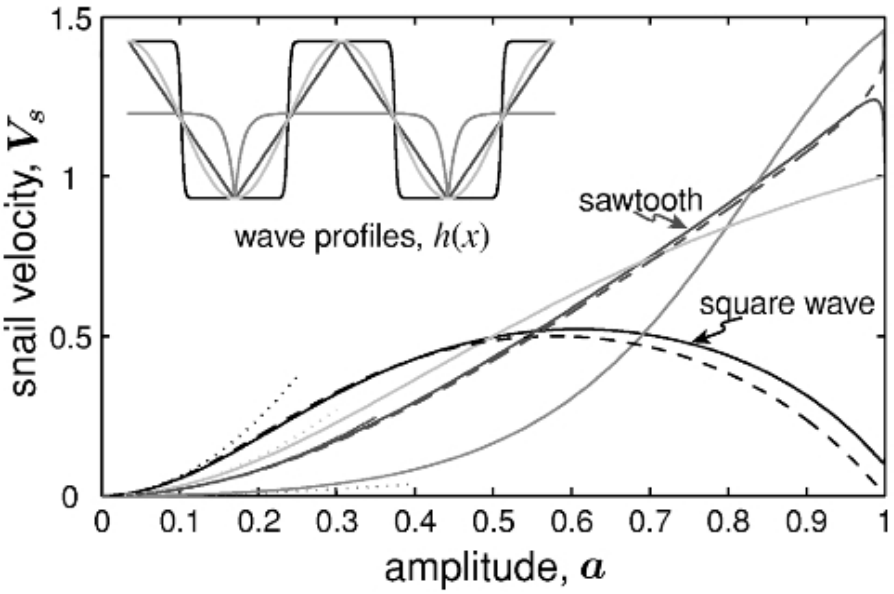

Figure 3-5: Free velocity behavior of robosnails using various wave shapes. The square wave performs favorably at low amplitudes, but as the amplitude nears $a = 1$, the sharper wave profiles gain an advantage. Note that the model predicts that certain wave shapes can achieve $\hat{V}_s > \hat{V}_w$.

3.2.2 Various wave shapes

As the equation shows, the force and velocity relation is a function of the height profile, which has been left in the general form $h(x)$. Thus any number of height profiles can be used, theoretically, resulting in a different force-velocity curve for each one. For the sinusoidal curve, or any shape curve, the first, easiest way to change the dimensionless height profile is to vary the amplitude with respect to the offset height. This is varied in the sections to follow. Figure **??**hows the dimensionless free velocity as a function of dimensionless amplitude for a variety of waving profiles. The most interesting piece of information is that for some profile shapes, such as the triangle wave, the expected snail velocity is greater than the waving velocity. This jump in snail velocity contradicts our intuition that the snail velocity should be some fraction of the waving velocity, no matter what.

To further understand the increase in speed due to sharp waveforms, we consider the interaction of the foot and the thin fluid layer. Upon close inspection, the extra "boost" in speed for the triangle wave arises near the lowest extremities of the waveform. When any the wave shapes approach the substrate, the pressure buildup and majority of propulsive force comes from the area immediately surrounding these minimum points. A snail with sinusoidal wave approaches the waving velocity as the waves near the substrate, but a snail having sharp waving profile should move even faster: near the touchdown points, the surface is much more sloped to take advantage of the pressures propelling the snail, furthermore, there is less surface in close proximity to the ground, so the shearing friction is greatly reduced.

To further explore this effect of sharp waveforms, we attempt to consider more waveform shapes besides the sinusoid and triangle wave. It makes the most sense to consider all wave-

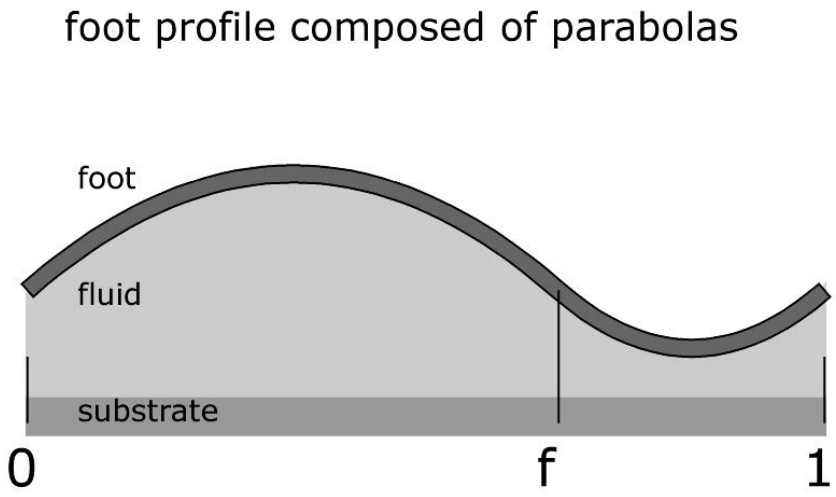

Figure 3-6: "composite" waveform made of two parabolas. By varing the sharpness factor f_s (the relative size of the first parabola to the entire wavelength) of the downturned parabola from near 0 to near 1, we can vary the free velocity as a function of the amplitude.

forms which have lower extremities that fall somewhere between the "smooth-bottomed" sinusoid and the "sharp-bottomed" triangle wave. Of course, there is an infinite number of wave shapes we can consider, as almost any arbitrary repeating shape can be made into a wave profile, at least in theory. However, it is the shape of the lower points that we are interested in, so we wish to find a wave type accordingly whose sharpness we can vary with ease. One simple solution is to replace the sinusoid with two parabolas, one opening upward and one opening downward. The advantages of this approach are that there are no slope discontinuities to disrupt the force equation, and we can indeed vary the sharpness by changing the sharpness factor f_s, the ratio of width of one parabola to the entire wavelength. As f_s approaches 1, the second parabola becomes nothing, and the waveform becomes an inverted parabola, repeating. While this is not exactly a triangle wave, it should behave much like one, since the low areas resemble the triangle wave, and the majority of the propulsive force is generated in this area. We would like to know at which f_s the snail starts to move faster than its own waving speed.

Since the velocity is a function of wave shape only, we use the velocity equation but instead of the sinusoid function we enter the parabola segment function and solve for free velocity as a function of the foot nearing the substrate (expressed as a variable amplitude A but defined for the irregular wave shape as $h_0 - h_{min}$ so that the geometry is normalized as with the sinusoidal case). The solution for free velocity as the foot approaches substrate, for various "sharpness ratio" f_s is shown in the figure 3-7. The "overdrive" phenomenon occurs roughly at a ratio of $f_s = 0.7$.

3.2.3 Three-dimensional effects for a finite-width snail

The two-dimensional theory is sufficient to explain how peristaltic motion of a membrane over a thin viscous fluid can propel itself. However, in most real-life situations requir-

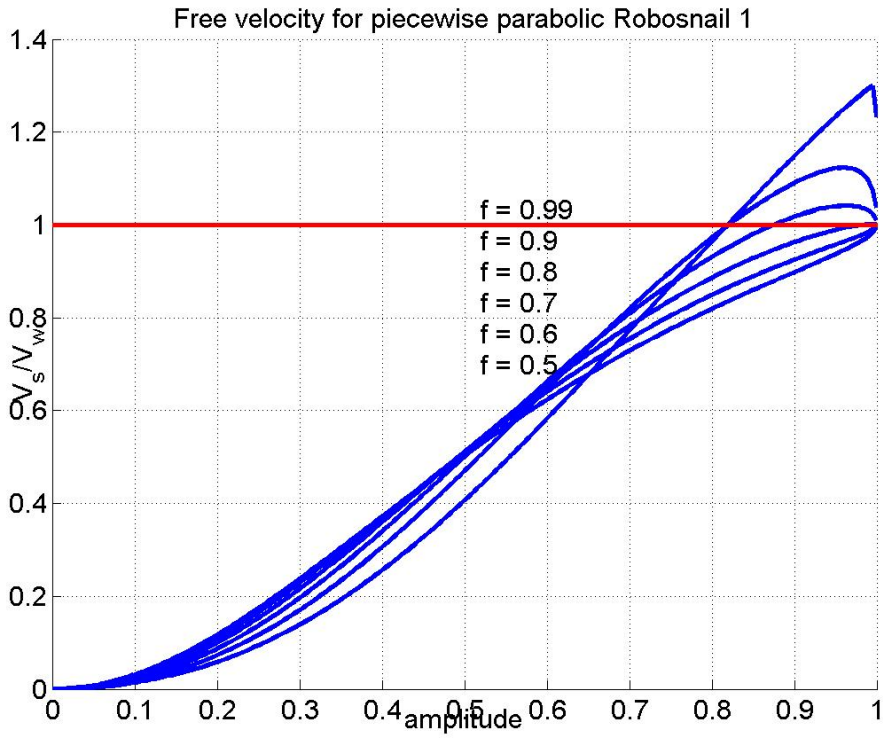

Figure 3-7: Dimensionless velocity as a function of the "sharpness ratio" of two parabolas. As one of the parabolas becomes less than 30 percent of the total wavelength, the snail begins to move at a speed greater than the waving speed $\hat{V_w}$.

ing robosnail-like motion, the snail has finite width, resulting in edge effects that cause a discrepancy between the two-dimensional and full three-dimensional results for force and velocity. At the edges of a finite-width waving sheet, the lubrication pressures built up underneath the waving sheet in regions near the substrate are diminished as fluid is allowed to leak to and from the outer region. Since the propulsive force is an integral of the pressure forces on the foot, we expect there to be losses in the expected pressure force. Meanwhile, we would not expect the shear losses due to forward motion to decrease as much, because shear stresses do not "leak" as pressure would. The overall expected result of imposing finite-width conditions would be decreases in the towing force, free velocity, and efficiency. This is verified by the and numerical simulations and experiments.

Due to the complexity of the three-dimensional flow in the gap of varying height, we found no analytical result to describe the pressure field under a finite-width sheet. However, we were able to numerically solve for the flow and pressure field using the three-dimensional lubrication equation, which, like the two-dimensional lubrication, remains valid as long as the Reynolds number is sufficiently low and the gap height sufficiently small compared to the wavelength.

In the simulation, the foot was divided into discrete segments, over one wavelength with boundary conditions of periodicity between the front and rear edges, and pressure falling to zero at the edge. The pressure force was found, as well as the net propulsive force, which is the integral of the pressure forces in the direction of travel. The velocity was solved in a manner analogous to the two-dimensional case. Figure 3-8 shows one characteristic plot of pressure over the surface of the foot.

The resultant force-velocity curves and pressure profiles were compared to the two-dimensional case, with identical amplitude and height parameters, and it the simulations predict that the finite width snails did not perform as well as the infinite case, matching our expectation. As we increase the snail width, the fluid has less opportunity to leak and the profile begins to resembles the 2D case. Figure 3-10 compares the ratio of stall force in 3D to the expected stall force in the 2D case while varying the foot width from near zero, two several times the wavelength. We see that for a given snail foot width, wave profiles that are closer to the ground have higher force closer to the 2D prediction compared to wave profiles that ride higher. Intuitively this makes sense as the fluid trapped in the small space between wave and ground would be less susceptible to leakage than the fluid underneath a larger space. At lower amplitudes of $0 < a < 0.1$, the snail's 3D to 2D force ratio remains virtually unchanged. This lower limit of force at low waving amplitudes suggests that the propulsive force is generated over a large area of the foot rather than concentrated spots along the low areas, and as the edge leakage affects the wider gap areas of the foot, the entire pressure field is affected by the leakage at these small amplitudes.

For all of the finite width cases (and with the later experiments), the analysis was done with the foot edges open to the fluid without any type of sealing. We expect a partial seal could be created with a wall that extended near to the substrate would be one way to hold in some of the pressure. We should expect some optimal separation between sealing wall and substrate where the pressure could be contained appreciably while the shear stress losses in the fluid gap between the edge of the sealing wall would not be to great as to nullify the benefits of the seal. Another way to improve performance, aside from building a wide snail, is to run the system inside a cylindrical environment, and to have the peristaltic motion of the foot generate waves in the axial direction inside the cylindrical hole (or around the outside of a cylindrical rod). This way, there will be no edge effects except the leading and trailing edges, and if the fluid layer is small in comparison with the rod, the fluid flow and

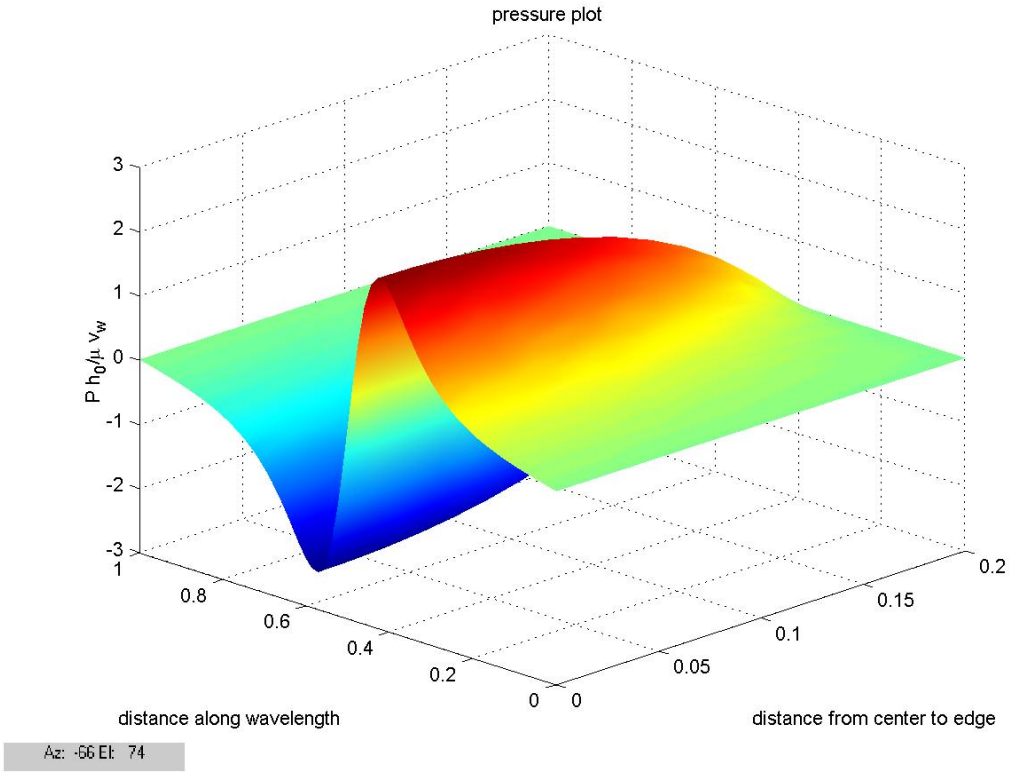

Figure 3-8: A typical Matlab simulation result of pressure underneath a finite width, periodic waving robosnail 1 foot. Only one side of a region of one wavelength long is shown. The simulation itself uses a periodic end conditions in x and is mirrored along the x-z plane. The waving foot generates a pressure similar to the two-dimensional waving robosnail foot near the centerline, but at the edges, the fluid is allowed to leak, and pressure decreases, decreasing the total propulsive force.

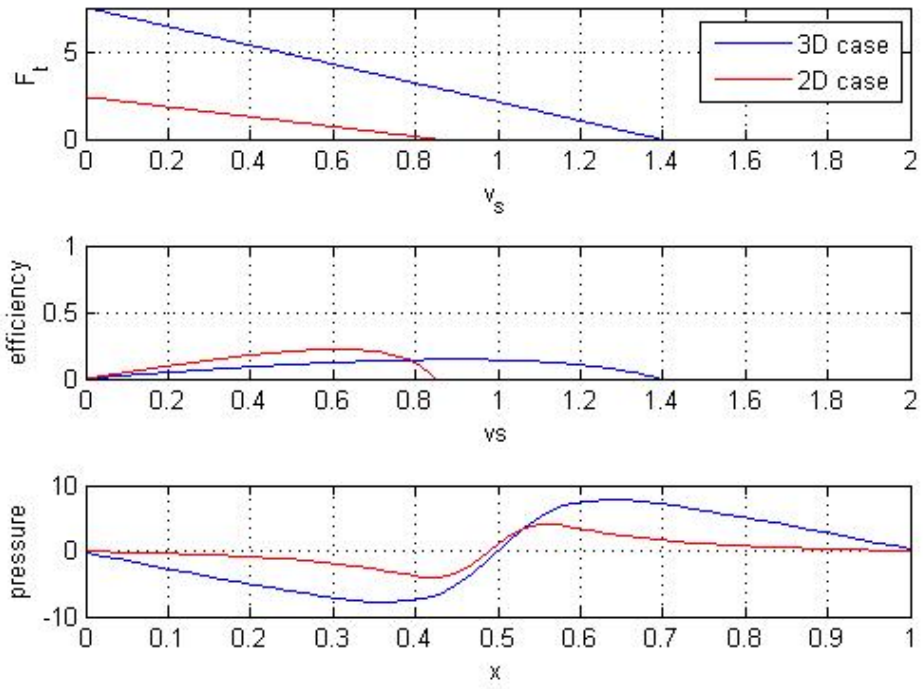

Figure 3-9: Tractoring force, snail velocity, and centerline pressure plot for robosnail 1, comparing a finite width snail of waving amplitude 0.8 times the wavelength, and a width equal to the wavelength with an infinitely wide snail. The wave shapes for both cases are the same. The finite snail suffers from edge leakage, which degrades the maximum tractoring force and velocities, as well as the efficiency. The centerline pressure serves as a qualitative evaluation of how much propulsive pressure is lost overall in the finite case.

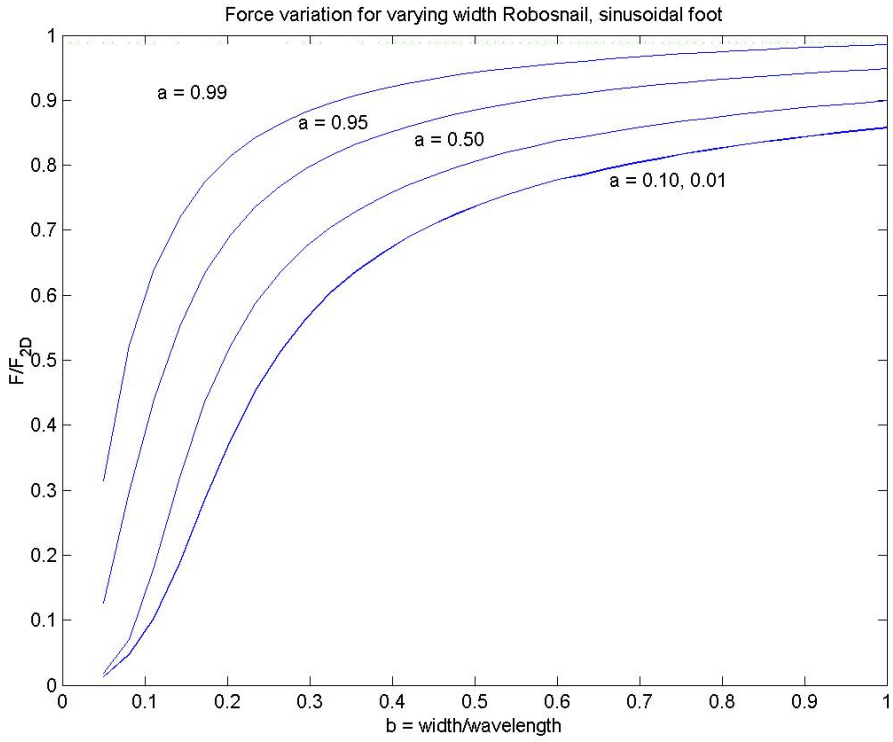

Figure 3-10: Simulation results showing ratio of tractoring force for a finite-width robosnail compared to the same robosnail 2D analytical result, with sinusoidal wave profile. Note that after $a < 0.1$ the expected force ratio follows the same curve.

forces can be analyzed using the 2D method.

3.2.4 Power and efficiency

The input power to a Robosnail device can be readily calculated with a simple integral. For every small section of foot, the differential amount of force exerted is equal to the pressure in the fluid times the differential area. For thin fluid layers, we can imagine the foot as being actuated by numerous small linear actuators, each feeling a resistance force of

$$dF = PdA = bPdx$$

the differential power exerted is the differential force times the vertical waving velocity at that point.

$$d\dot{W} = V_y dF = V_y bPdx$$

.

$$\dot{W} = b\int_0^L V_y Pdx$$

Recall, however, that $V_y = V_w \frac{dh}{dx}$, so that

$$\dot{W} = V_w b\int_0^L \frac{dh}{dx} Pdx$$

Since $F_{x,P} = b\int_0^L \frac{dh}{dx} Pdx$, the power expended simplifies to the expression

$$\dot{W} = V_w F_{x,p} \tag{3.10}$$

The efficiency of the snail is the ratio of useful power to the power expended:

$$\eta = \frac{\hat{V}_s F_t}{\hat{V}_w F_{x,P}} = \frac{V_s f_t}{f_{x,p}} \tag{3.11}$$

In the 2D case, we can substitute the expressions for the horizontal pressure force 3.6 and snail velocity 3.7 to find an analytical expression for the efficiency as a function of snail velocity:

$$\eta_{2D} = \frac{I_1 V_s[6(1-A) - V_s(4-3A)]}{\left[12I_1 - \frac{I_2^2}{I_3}\right]\left[1 - \frac{V_s}{2}\right]} \tag{3.12}$$

In three dimensions, the snail velocity and pressures can be found numerically. Figure 3-9 compares the efficiency for a the 2D case and a typical 3D case, where the snail width is 0.8 times the wavelength. The wave shapes for both cases are the same. The finite-width snail generally experiences a lower efficiency than its 2D counterpart, as we had expected.

3.3 Mechanisms

The most basic wave that can be generated with the waving foot is a sinusoidal wave. To do this, we used a shallow helix threaded through slotted plates which are constrained to move vertically. The bottom edges of the rectangular plates are affixed to a flexible membrane. Each of the plates then acts as a connecting rod, with its section of helix acting

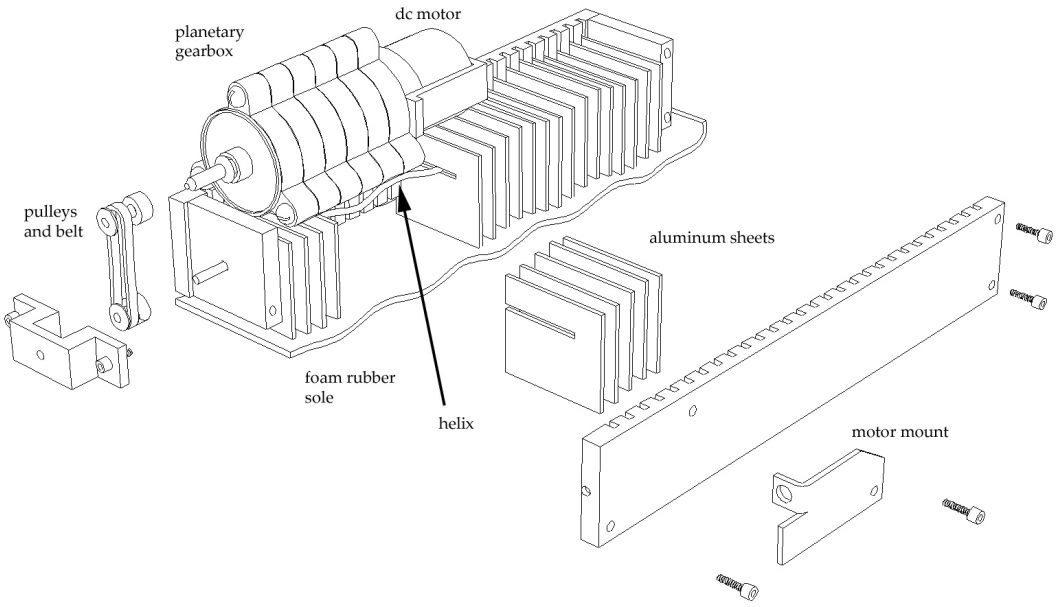

Figure 3-11: Partially exploded view of Robosnail 1 showing motor/gearbox assembly, rotating helix, slot plates, and membrane.

as a crank, transferring the vertical component of its rotational motion to its part of the membrane. The helix, thus acting as a crank, was driven by a heavily geared-down motor. The resultant motion of the rotating helical crank is a traveling sinusoid along the length of the membrane. The wave speed is simply equal to the wavelengths divided by the rotations per second.

A handful of designs were proposed for the construction of a peristaltic robosnail that could mimic any waveform, but of the few that were built ultimately none of the designs tested were reliable enough to generate useful data. One of the main difficulties was to create a device with high enough resolution to emulate the sharp waveforms that are of the most interest. Many of the devices required a large number of linkages each connected to a cam follower, but the complexity of the systems made construction of such devices difficult. However, they are included in here for the sake of discussion and completeness.

One cam-driven robosnail that was actually built (3-12 involved an interchangeable cam which could accommodate up to 64 cam followers. The membrane was wrapped around in a circle concentric with the cam, so the motion of the snail (actually the fluid, as the tank was made rotatable) was in a circle concentric with the rest. This was done for two reasons, to simplify the machine enough so it could be built, and to make the waveform truly periodic. As long as the width of the snail was small enough compared to the mean diameter of the membrane, we could still compare the results to the 2D theory. The experiment yielded little useful data, as the membrane was barely wide enough to generate force, so the tank rotated much less than the 2D prediction. The snail was invented and prototyped at a time when the 3D theory was still being formulated. Later on, more of the 3D theory and experiments were finalized, and showed that we had been operating at such a low aspect ratio of width vs. wavelength, that only a small velocity and force would be measurable compared to what the infinite-width snail would have generated. The effect of the pressure

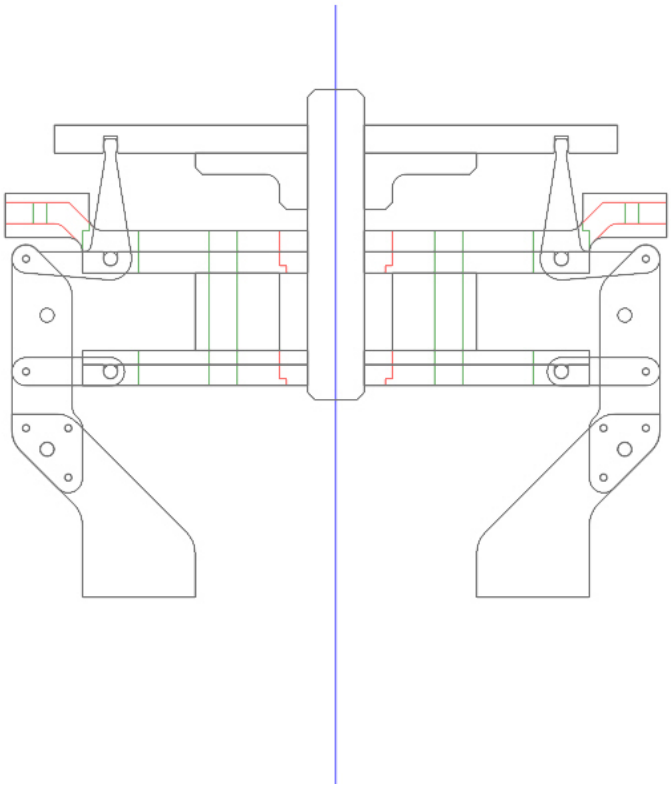

Figure 3-12: Side cross-section of the "ring snail" with interchangeable cams

leakage from the sides removed almost all propulsive force. What further complicated the analysis was that the tank walls inhibited some of the pressure loss, so while the snail was far from the ideal infinite case, the results could neither be directly compared to the 3D simulations, which described a free fluid with no side walls. The snail suffered from high friction at the cam followers, even with only 8 followers installed; this suggested that a larger number of followers would likely result in unpredictable outputs.

Another proposed method to generate arbitrary waveforms was to use a semisolid belt with waveform "chunks" attached on the outer surface. The belt would run against a stretched membrane so that its shape would be transferred onto the membrane while the surface of the membrane would remain more or less at a constant place rather than being pulled along with the belt. A similar idea involved using screwlike rollers to transfer a sharp trough wave profile onto a membrane with lateral stiffness members. (see figure 3-14) As all of these proposed devices involved rubbing of a tensioned membrane against a moving form, we doubted that we could build an effective device with enough tension in the membrane to hold it against the form to counteract the high pressures at the wave troughs, while having a low enough friction between the moving form to run reliably. The conclusion was that a system using cams and actuators would likely be more efficient albeit harder to construct.

In the end, the helix-driven sinusoidal robosnail 1 models were the most reliable versions and will be the focus of this study.

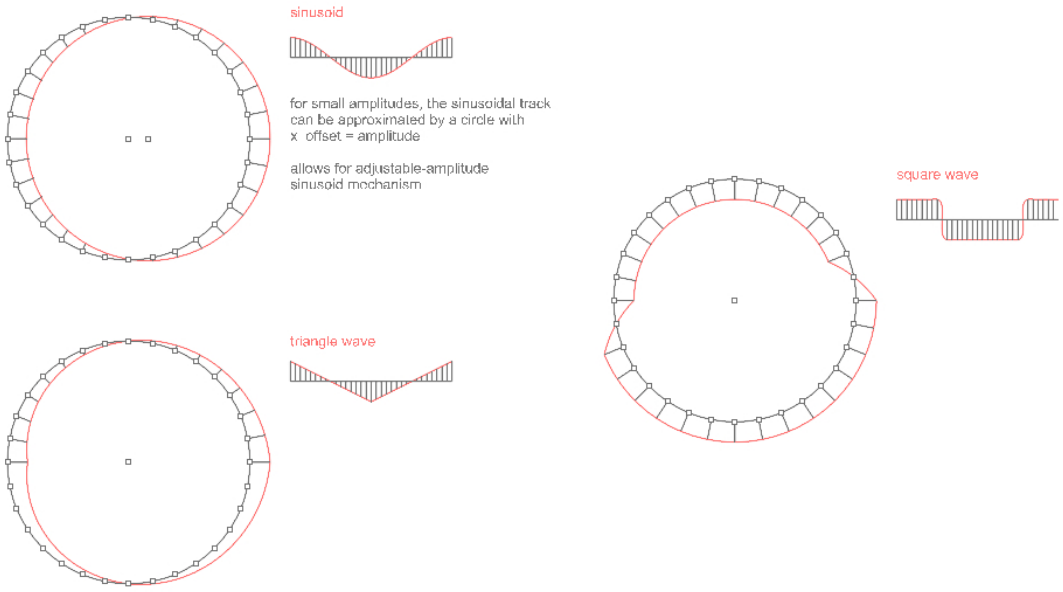

Figure 3-13: Some interchangeable cams that would allow various wave shapes for the ring/periodic robosnail 1.

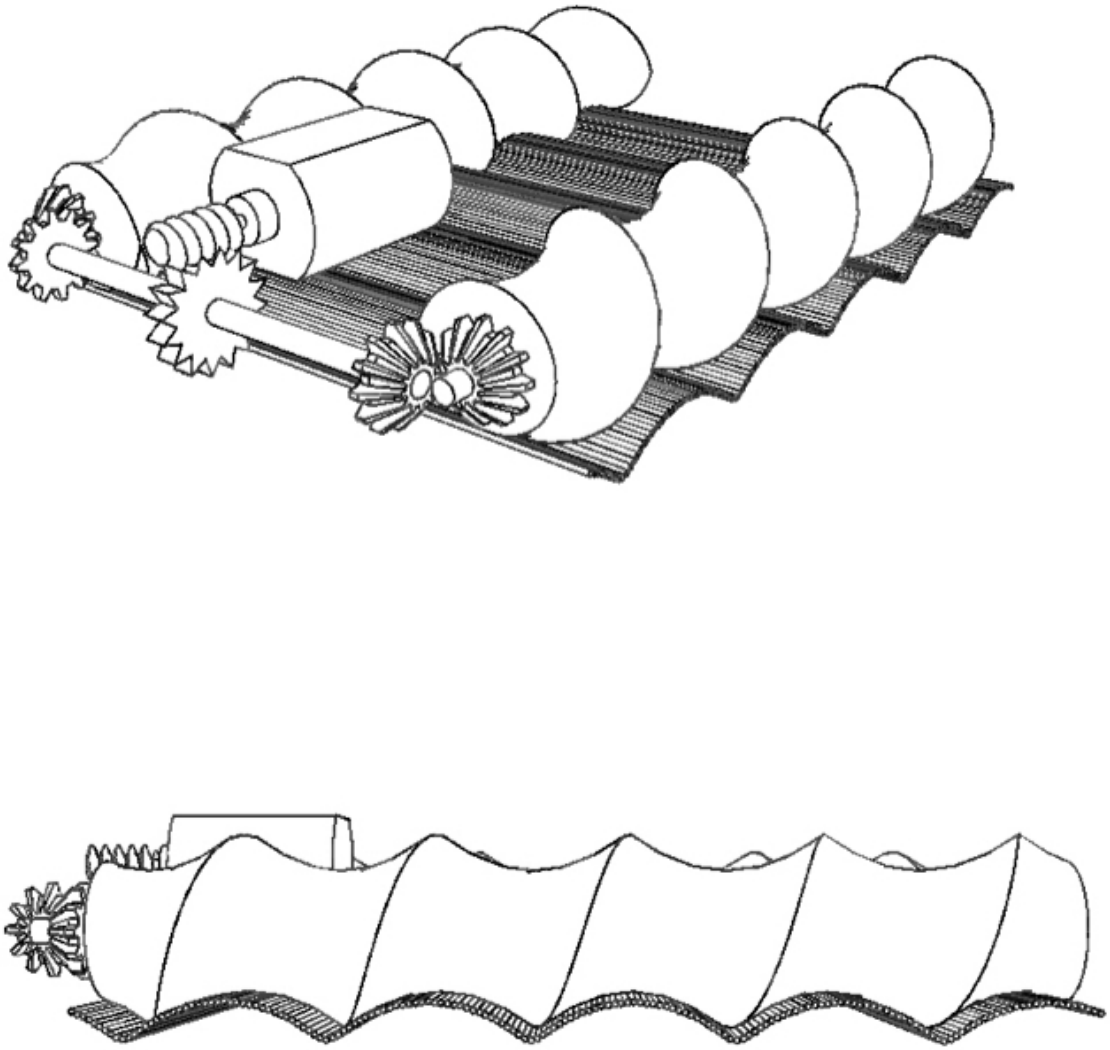

Figure 3-14: Another robosnail 1 type design for generating a non-sinusoidal waveform in the membrane. This particular design aims for the "overdrive" phenomenon where the snail velocity exceeds its own waveform velocity. The membrane is reinforced with lateral stiffness members, and is stretched across two spiral cams. The motion of the

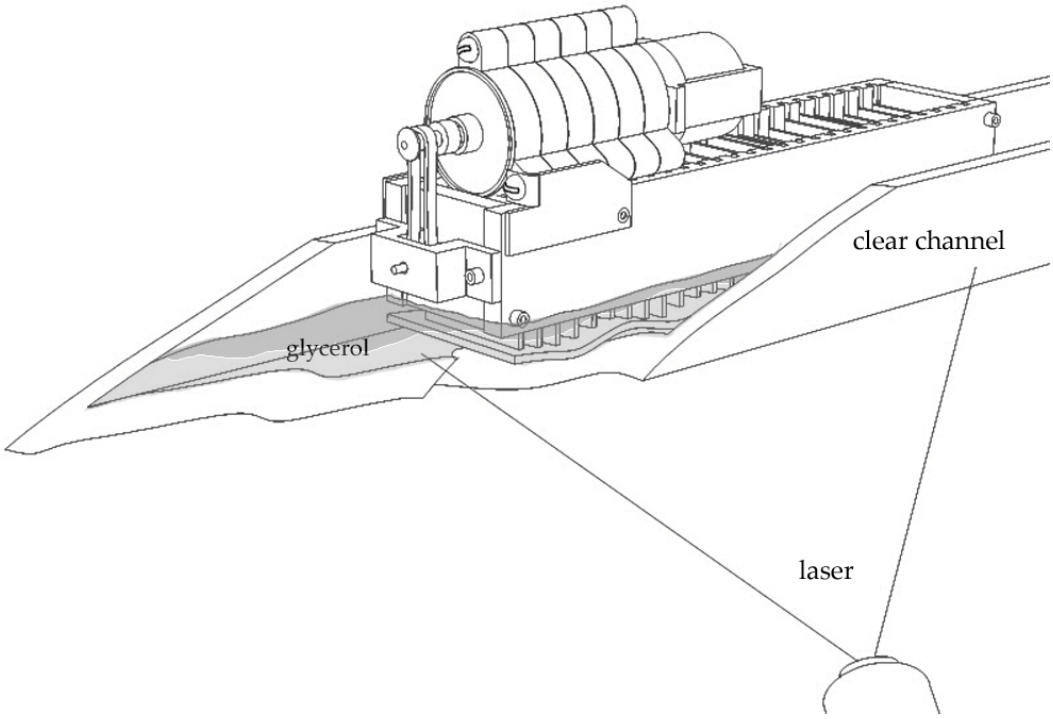

Figure 3-15: Setup for measuring free velocity for robosnail. The channel contains the working fluid, enough to submerge the entire foot so that the peristaltic motion does not entrain air bubbles during operation. The laser sheet shone at at angle onto the bottom foot surface, so that the profile could be measured and the wave profile and fluid thickness could be determined.

3.4 Experiment

Several experiments were conducted to confirm the analytical and numerical results. As we have seen already, many wave shapes result in different force or velocities, and conceivably many other waves can be experimentally analyzed for their behavior. Due the difficulty of constructing a device to generate custom waveforms, we only collected data for the sinusoidally waving robosnail. The experiments were mainly to confirm that the theory predicting force and velocity were reliable.

The first experiment was to test the free velocity of the snail without pulling any load. The snail was run in a pan of glycerol for some tests, later switching to silicone oil (the hydroscopic quality of glycerol varied its viscosity from day to day, introducing unwanted experimental errors). The snail was first tested without any support - it was allowed to sink freely into the liquid, then run to find the free velocity as the foot neared the substrate. In later experiments the snail was placed on a track which held the snail at a constant height from the substrate. Later experiments also involved a stationary force experiment to test the stall force of the waving robosnail at various heights and a moving force experiment (3-16), where various tractoring forces were applied to a waving robosnail, and the resultant velocity was measured.

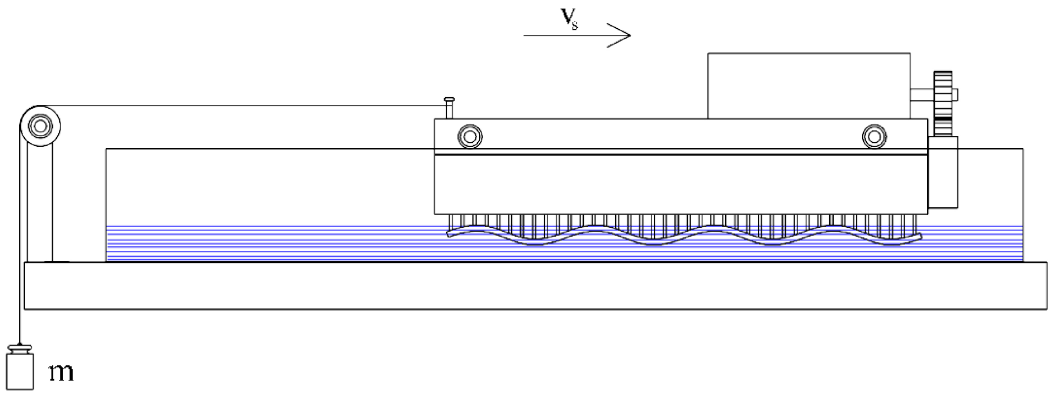

Figure 3-16: Setup for measuring the moving tractoring force of the snail. Small support wheels on tracks hold the snail at a fixed height from the substrate, while the pulley setup allows the payload to be easily adjusted.

3.5 Results and Discussion

It was found that the snail performed very much according to the predictions made by theory and numerical data. First, it was confirmed (figure 3-17) that the free snail velocity is proportional to the waving velocity when geometry and other variables were held constant.

The second test conducted was the stationary tractoring force, which we also expect to be proportional to the waving velocity. The data agreed very closely with the numerical result (figure 3-18).

The last set of data was to confirm the linear tradeoff relationship between tractoring force and waving velocity. The snail was operated at various waving speeds and the tractoring velocity was measured as it pulled loads of varying sizes. The load was increased and the tractoring force was found to drop linearly (3-19) as the theory predicted.

The last set of data describing the tractoring force varied slightly from the theoretical value in the slope of the force-velocity curve. The experiment found a greater tractoring force for higher payloads, and a smaller tractoring velocity near the zero-payload free moving range. The most likely explanations for this discrepancy is that at low speeds, the fluid buildup behind the stalling robosnail resulted in an increase in hydrostatic pressure pushing against the snail in its favor. At high speeds, oil friction in the bearings probably caused the steeper drop-off in performance. Despite this small deviation from the expected performance, the results show a close enough correlation to the theory that we can be fairly confident that the theory and numerical results represent an accurate model of persistaltic locomotion.

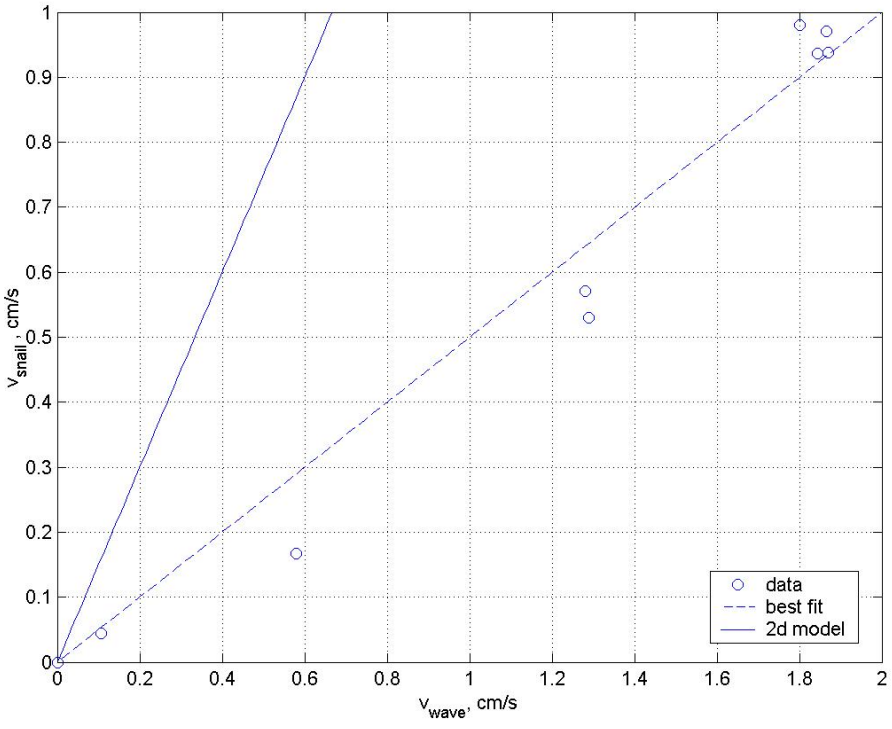

Figure 3-17: Free velocity of robosnail plotted against waving velocity. Fluid is silicone oil.

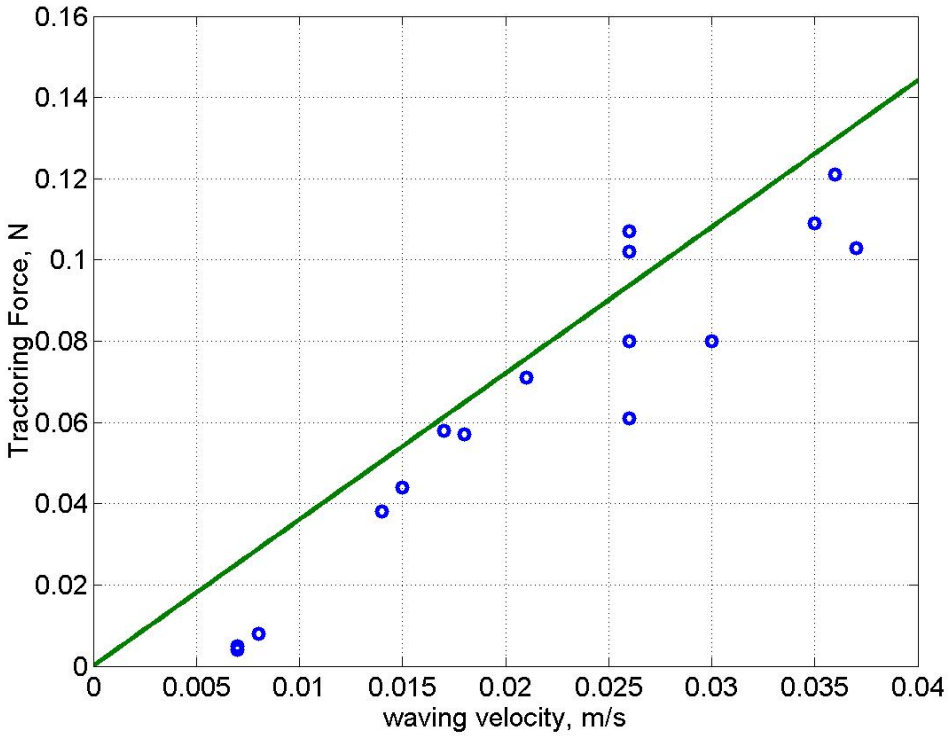

Figure 3-18: Tractoring force of Robosnail 1, plotted against waving velocity. The resultant tractoring force is linearly proportional with respect to waving velocity, as expected. The solid line represents the corresponding tractoring force predicted by numerical results for a snail of aspect ratio $b/l = 0.6$ with a sinusoidal wave amplitude ratio of $a/h = 0.7$. Fluid is silicone oil.

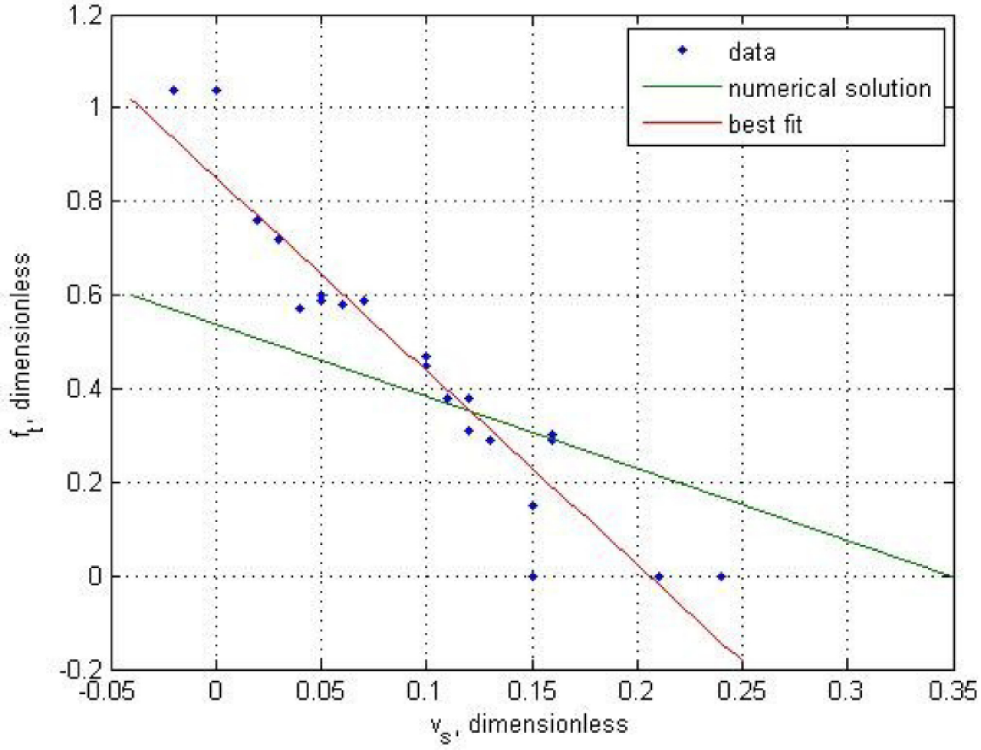

Figure 3-19: Force-velocity data for Robosnail 1. The payload force was increased while the robosnail velocity was measured. The snail velocity decreased linearly as expected. Fluid is silicone oil. The foot aspect ratio is aspect ratio $b/l = 0.6$, with a sinusoidal wave amplitude ratio of $a/h = 0.7$.

Chapter 4

Robosnail 2

4.1 Introduction

After producing Robosnail 1, we were motivated to develop a machine and fluid system capable of climbing walls and ceilings like real snails (Robosnail 1 only was effective at moving over surfaces that were smooth and horizontal). With this goal in mind our continued research after Robosnail 1 led to the creation of Robosnail 2. After reviewing several studies on land-snail locomotion, we found that most of the snails that were examined moved by adhesive locomotion, where propulsive forces are through fluid shear, not pressure forces as in the case of Robosnail 1.

While Robosnail 1 is capable of moving through viscous fluids, it possesses several limitations. Real snails are known for their ability to traverse vertical and inverted planes, thus highlighting an important feature of snail mucus - finite yield stress. Robosnail 1, which is designed to run on Newtonian liquids, cannot climb walls unless it is completely submerged, due to the consequence of a Newtonian fluid flowing down and out of the gap by the force of gravity. Even if it were submerged in a viscous fluid, a Robosnail 1 robot would require some sort of active pumping mechanism to keep itself adhered to the wall using fluid pressure, while real snails can adhere to a wall even when their foot is immobile. The benefits of Robosnail 2 mirror those of real snails in more ways than one: by using a non-Newtonian shear-stress fluid, Robosnail 2 can generate more force whether stationary or mobile, than Robosnail 1 (per unit of foot area) and was found to be more efficient than Robosnail 1.

Robosnail 2 will likely prove to be a useful proof-of-concept for later machines that operate in environments with highly non-Newtonian fluids. The bodies of organisms, oil drilling sites, lake bottoms, and other muddy environments are a few examples where snail-like locomotion might be advantageous.

4.2 Theory

At first glance, both Robosnails appear very similar: they are both mechanisms with a flexible foot, and they propel themselves over a thin lubrication layer of fluid using cyclical undulations of the foot. Despite these similarities, the two versions are fundamentally very different. While Robosnail 1 relies on high lubrication pressures to propel itself, Robosnail 2 is propelled by the shear forces within the fluid film, and pressure forces are negligible. Furthermore, Robosnail 1 was built for use with a viscous newtonian fluid, while Robosnail

2 requires a non-Newtonian fluid to move forward, and, as we will show later, does not function with a Newtonian fluid at all.

The phenomenon of adhesive locomotion, as its name implies, is one of selective gluing and ungluing of an actuated membrane onto a substrate. In this illustration, the mucus acts as the glue. Unlike an ordinary glue, however, the mucus can be switched from solid to liquid states when subjected to a sufficient amount of shear force. This is essential in order that the snail can undergo a net motion. If the snail then generates standing traveling compression waves from one end of the membrane to another, such that the fluid beneath waves is sheared to to the point of yielding, then the snail is able to travel forward incrementally with each new wave. As long as the fluid beneath the areas between compression waves (the interwaves) does not shear past the critical yield stress, the snail moves forward without slip. One final, necessary requirement of the fluid is that it be able to re-solidify (or restructure) after yielding; if this were not the case,

4.2.1 Physics

A snail of this type has a flat foot, with a mucus layer of fixed height, whose surface deforms with an time-dependent displacement

$$u = u(\hat{x}, t)$$

where the deformation u is the displacement of a point on the foot from its average position. For our purposes, u is constrained to the horizontal plane in the $x-$ direction. We limit our analysis to traveling waves of a fixed shape

$$u = (\hat{x} - \hat{V}_w t) \tag{4.1}$$

which are periodic such that

$$u(\hat{x}) = u(\hat{x} + \lambda)$$

and defined such that the average deformation is zero:

$$int_0^{\lambda} u dx = 0$$

At this point it is important to know the strain in the foot

$$\epsilon = \frac{\partial u}{\partial x}$$

which in gives us the foot compression ratio

$$\frac{dx'}{dx} = 1 + \frac{\partial u}{\partial x}$$

The snail itself is moving at a velocity $\hat{V}_s$ so that the net velocity of a point is the sum

$$\hat{V}_p = \dot{u} + \hat{V}_s$$

Applying 4.1,

$$\hat{V}_p = \hat{V}_w \frac{du}{dx} + \hat{V}_s$$

The net force on the foot is equal to the tractoring force, and is the integral of all the shear forces on the foot,

$$\hat{F}_t = \int \tau dA$$

for a snail of width b and length L,

$$\hat{F}_t = b \int_0^{\lambda} \tau \left(1 + \frac{\partial u}{\partial x}\right) dx \tag{4.2}$$

if the fluid is described by some viscosity μ

$$\hat{F}_t = b \int_0^{\lambda} \mu \frac{\hat{V}_p}{h} \left(1 + \frac{\partial u}{\partial x}\right) dx \tag{4.3}$$

$$\hat{F}_t = b \int_0^{\lambda} \mu \frac{\hat{V}_w \frac{du}{dx} + \hat{V}_s}{h} \left(1 + \frac{\partial u}{\partial x}\right) dx \tag{4.4}$$

Equations 4.3 and 4.3 describe the force-velocity relationship for any snail using in-plane foot deformations to move on a thin layer of fluid.

4.3 and 4.3 carry several conditions which we assume to be valid: first, that the pressure gradient $\frac{dp}{dx}$ is negligible and therefore that the velocity profile in the fluid gap is linear. For these conditions to hold for an incompressible fluid, we must assume that the foot height h must change with x in order that fluid mass be conserved. However, we will assume that this change in h is small. Finally, the flow and the snail motion are assumed to be steady-state, so that inertial forces are negligible. The viscosity μ in this case is understood to be variable. In most cases described herein, viscosity is a function of shear rate $\dot{\gamma} = \frac{dv_x}{dy}$ but can be vary according other factors depending on the type of fluid used. It can be shown[1] when a Newtonian fluid is used, in-plane foot motions cannot create a propulsive force; therefore, a non-Newtonian fluid is required for robosnail 2 to function.

[1]When this is the case, equation 4.4 becomes

$$\hat{F}_t = \frac{\mu b}{h} \int_0^{\lambda} \left(\hat{V}_w \frac{du}{dx} + \hat{V}_s\right) \left(\frac{\partial u}{\partial x} + 1\right) dx$$

$$\hat{F}_t = \frac{\mu b}{h} \int_0^{\lambda} \left[\hat{V}_w \left(\frac{du}{dx}\right)^2 + \left(\hat{V}_w + \hat{V}_s\right) \frac{du}{dx} + \hat{V}_s\right] dx$$

$$\hat{F}_t = \frac{\mu b}{h} \left[\int_0^{\lambda} \hat{V}_w \left(\frac{du}{dx}\right)^2 dx + \int_0^{\lambda} \left(\hat{V}_w + \hat{V}_s\right) \frac{du}{dx} dx + \int_0^{\lambda} \hat{V}_s dx\right]$$

$$\hat{F}_t = \frac{\mu b}{h} \left[\hat{V}_w \int_0^{\lambda} \left(\frac{du}{dx}\right)^2 dx + \left(\hat{V}_w + \hat{V}_s\right) u|_0^{\lambda} + \lambda \hat{V}_s\right]$$

since the deformation is periodic, $u(\lambda) = u(0)$, the second term within the brackets goes to zero

$$\hat{F}_t = \frac{\mu b}{h} \left[\hat{V}_w \int_0^{\lambda} \left(\frac{du}{dx}\right)^2 dx + \lambda \hat{V}_s\right]$$

However, for small strains of the foot $\frac{du}{dx}$, $\left(\frac{du}{dx}\right)^2$ is small and the remaining integral is negligible. The remaining result

$$\hat{F}_t = \frac{\mu b}{h} \lambda \hat{V}_s$$

is independent of waving speed, and is only the viscous drag one would expect from dragging a membrane through a viscous fluid, regardless of whether or not the membrane was deforming.

The force F is the net tractoring force, equal to the propulsive force exerted by the foot of the snail.

To simply the theoretical problem and the mechanical solution, we consider a Robosnail composed of a foot divided into two discrete, uniform sections which can each be considered to be uniform. We assume that the waves and interwaves are respectively of area A_w and A_i and move at steady velocities v_w and v_i. The net force integral can then be calculated as a product of shear stresses and their corresponding areas. Besides simplifying the analysis, this model can be achieved mechanically by constructing a foot consisting of n segments, and to employ a sliding pattern in which only $\frac{1}{7}n$ section is moving at v_w while the remaining segments move at $-v_i$.

We use a force balance to analyze the snail locomotion in steady state. The foot is separated in two parts: the wave and the interwave. The forces on the interwave and wave are :

$$F_i = A_i \tau_i = A_i \mu_i \dot{\gamma_i}$$
$$F_w = A_w \tau_w = A_w \mu_w \dot{\gamma_w}$$

for the thin, constant thickness layer,

$$F_i = A_i \mu_i \frac{\hat{V_i} - \hat{V_s}}{h_0}$$
$$F_w = A_w \mu_w \frac{\hat{V_w} - \hat{V_s}}{h_0}$$

Because the waving motion is prescribed by the mechanism design, the wave and interwave velocities $\hat{V_w}$ and $\hat{V_i}$ are measured with respect to the snail while v_{cm} is measured in the lab frame. The sum of forces equal the tractoring force in steady state,

$$F_i + F_w = F_t$$

The average velocity of any segment must equal zero with respect to the snail, $\frac{1}{\lambda}\int_0^\lambda \hat{V} dx = 0$ which results in

$\hat{V_i} = -\frac{\hat{V_w}}{N-1}$, therefore

$$F_t = \frac{A}{N h_0}[\hat{V_w}(\mu_i - \mu_w) - \hat{V_s}(\mu_i(N-1) + \mu_w)]$$

This is the general equation for tractoring force given a Robosnail 2 mechanism configuration (N discrete pads moving with wave and interwave speeds). The result tells us that movement of the pads cannot generate thrust when the viscosity of the fluid is constant (Newtonian fluids)- the only force that occurs is viscous friction if the snail is being dragged. The viscosity of the fluid in the interwave must be greater than the fluid in the wave for the foot motion to create any positive tractoring force, and this is the case with real snails. We can conclude from this result that the thrust would be forward for a shear-thinning fluid, and backward for a shear-thickening fluid, where the viscosity in the slow interwave would be less than that in the faster moving wave.

It can be shown[2] that for the discrete interwave/wave model with described above, the foot cannot apply a net force on the substrate if the gap is filled with a Newtonian fluid. If, however, the fluid is a Bingham fluid (or any fluid that exhibits a shear stress that is not linear with shear rate), the behavior is different. In the following model we assume that the fluid has not yielded underneath the interwave (A condition we are trying to maintain).

The tractoring force and resultant speed of the snail highly dependent on the viscosity function of the fluid, and many results can be found using different types of non-Newtonian fluids. It is important to keep in mind that the viscosity of non-Newtonian fluids depends on the shearing rate itself, therefore evaluating the force equation is often nontrivial. The Bingham fluid approximation provides certain simplifications which yield a useful analytic result.

4.2.2 Bingham fluid approximation

One practical non-Newtonian fluid is the Bingham fluid, which is similar to Newtonian fluids in that it the stress increases proportionally with strain rate, the only difference being that a certain yield stress needs to be exceeded before the fluid starts to flow. Many clays can be behave like Bingham fluids and are well approximated by the model. We can apply a similar force-balance analysis as shown above using a Bingham fluid as lubricant.

We assume a Bingham fluid model for the non-Newtonian fluid filling the gap of uniform thickness h_0. The total contact area is A, divided into N discrete sections. Recall from the Robosnail 2 model that at all times, $\frac{1}{N}$ of the area of the foot is moving upward with a speed of V_w while the rest of the $\frac{N-1}{N}$ segments are moving downward with a speed of $\frac{-\hat{V}_w}{N-1}$. We will refer to these two areas of the foot the wave and interwave, respectively. With respect to the substrate, the wave moves forwards at $\hat{V}_w - \hat{V}_t$ and the interwave moves backwards with $\frac{-\hat{V}_w}{N-1} - \hat{V}_t$. (Note that we desire $\hat{V}_t$ to be usually negative.

Note the Bingham number

$$Bin = \frac{\tau_y h_0}{\mu \hat{V}_w} \tag{4.5}$$

which is the ratio between the yield stress and the Newtonian fluid stress in the fluid. Essentially, a larger BIngham number corresponds to a greater deviation from Newtonian behavior, where the limit of $Bin = 0$ corresponds to zero yield stress and a Newtonian fluid. The stress under the interwave τ_i will be rewritten as:

[2]When this is the case, the fast moving smaller section experiences a force of

$$F_{wave} = \mu \frac{A(V_w - V_t)}{N h_0}$$

The slow moving interwave section feels an opposing force of

$$F_{interwave} = \mu \frac{A(N-1)(-\hat{V}_i + \hat{V}_t)}{N h_0} = \mu \frac{A(N-1)(-\hat{V}_w/(N-1) - \hat{V}_t(N-1))}{N h_0}$$

The total fluid force exerted on the tool is then

$$F = \mu \frac{A(\hat{V}_w - \hat{V}_t) + A(-\hat{V}_w - \hat{V}_t(N-1))}{N h_0} = -\mu \frac{A\hat{V}_t}{h_0}$$

When we consider the a snail without tractoring force, the forces from foot motion exactly balance, and the net force is due to the relative motion of the snail, $\hat{V}_t$. The snail will drift with a constant velocity independent of $\hat{V}_w$.

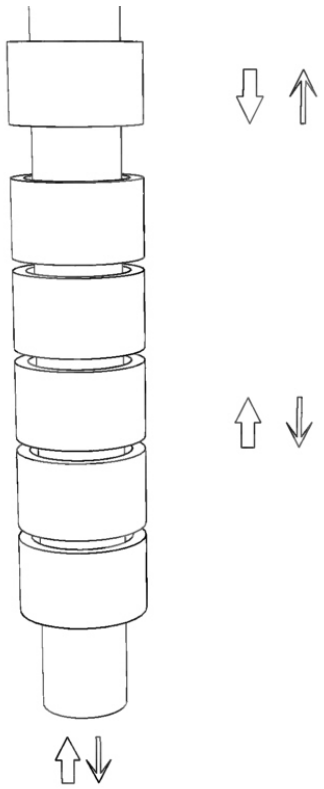

Figure 4-1: Force balance on a cylinder being conveyed using a Robosnail type-2 mechanism, without slip.

$$\tau_i = f_s \tau_y$$

Where f_s is a shear factor, or the fraction of the yield stress which is reached beneath the interwaves. For there to be no slip locomotion, we intend that $f_s < 1$. We will define a safety factor $S = \frac{1}{f_s}$ to fit the standard engineering convention. The force balance on the snail: On the wave: $F_w = (\tau_y + \frac{\mu(V_w+V_t)}{h_0})\frac{A}{N}$ On the interwave $F_i = f_s\tau_y\frac{N-1}{N}A$ On the bottom face $F_t = PA_c$

$$F_i = F_t + F_w$$
$$f_s\tau_y\frac{N-1}{N}A = PA_c + (\tau_y + \frac{\mu(V_w+V_t)}{h_0})\frac{A}{N}$$

Solving for tractoring force:

$$F_t = PA_c = \frac{A\tau_y}{N}(f_s(N-1) - \frac{1}{Bin}\frac{N}{N-1} - 1) \tag{4.6}$$

The maximum force the tool can sustain without slipping is when $f_s = 1$ and $\tau_i = \tau_{yield}$. As long as the condition holds, there is no slip and the interwave velocity with respect to the tool is zero

$$V_i - V_t = \frac{-V_w}{N-1} - V_t = 0$$

and the tractoring velocity can be solved:

$$V_t = V_i = -\frac{V_w}{N-1}$$

.

4.2.3 Motion with slippage

Once τ_i increases beyond τ_{yield}, the foot slips, and the forces in the wave and interwave are both functions of the yield stress and the tangent viscosity.

$$F_w = \frac{A}{N}(\tau_y + \mu\frac{V_w + V_t}{h_0})$$

$$F_i = \frac{(N-1)A}{N}(\tau_y + \mu\frac{\frac{V_w}{(N-1)} - V_t}{h_0})$$

defining $v_t = \frac{V_t}{V_w}$

The force balance with slippage:

$$F_t = \frac{A}{N}\tau_y[N - 2 - \frac{Nv_t}{Bin}]$$

Which takes has a linear force-speed curve similar to Robosnail 1. Note that even with slippage, there is a net motion.

4.2.4 Power and Efficiency

Once the force and velocity relations are well defined, finding the power requirement is straightforward. The total power consumed is the sum of the power required to move the interwave and the power required to move the wave, while the useful power output is the product of the tractoring force and the tractoring velocity.

$$\wp = \sum_j F_j v_j = F_{wave} V_{wave} + F_{interwave} V_{interwave}$$

$$\eta = \frac{F_t V_t}{\wp}$$

By substituting the equations for force and tractoring velocity, we arrive at the following expressions for the power and efficiency:

Without slip:

$$\wp = \frac{A}{N} \tau_y V_w [1 + f_s + \frac{1}{Bin} \frac{N}{N-1}]$$

$$\eta = \frac{f_s - \frac{N}{Bin(N-1)^2} - \frac{1}{N-1}}{1 + \frac{N}{Bin(N-1)} + f_s}$$

With slip:

$$\wp = \frac{A}{N} \tau_y V_w [2 + \frac{1}{Bin} \frac{N}{N-1}]$$

$$\eta = \frac{(N - 2 - \frac{N v_t}{Bin}) v_t}{2 + \frac{N}{Bin(N-1)}}$$

Notice that as f_s approaches 1, the power and efficiency expressions of the no-slip case approach that of the slip case.

We can see that for higher Bingham numbers, a higher efficiency is possible. This makes sense because high Bingham numbers represent a greater deviation between apparent viscosities of the working fluid, while at lower Bingham number, the setup more resembles the Newtonian case, which we have already proven cannot generate a tractoring force and hence exhibits zero power output. For each efficiency curve, the curve intercepts the x-axis at a nonzero f_s; this is the point at which the snail starts moving, and before which a forward F_t must be applied for the snail to be moving in the correct direction; the negative required input power results in a negative efficiency. The highest efficiency occurs when $f_s = 1$. Efficiency decreases quickly at higher f_s since any additional forces would be to overcome viscous friction. Efficiency again falls to zero after a certain value of $f_s > 1$; this is where the interwave exerts just enough force to sustain the drag force of the wave.

4.3 Mechanical Design

An early incarnation **??** of Robosnail 2 employed N foot pads independently actuated by lengths of Nitinol "muscle wire". The prototype, which used an external power source, was lightweight enough to climb walls and move upside down using a thin layer of Laponite suspension. However, our dissatisfaction with the complexity of the control, the slow restructuring time and low yield stress of the Laponite, and resultant small maximum size of robosnail led us to continue development of an improved version.

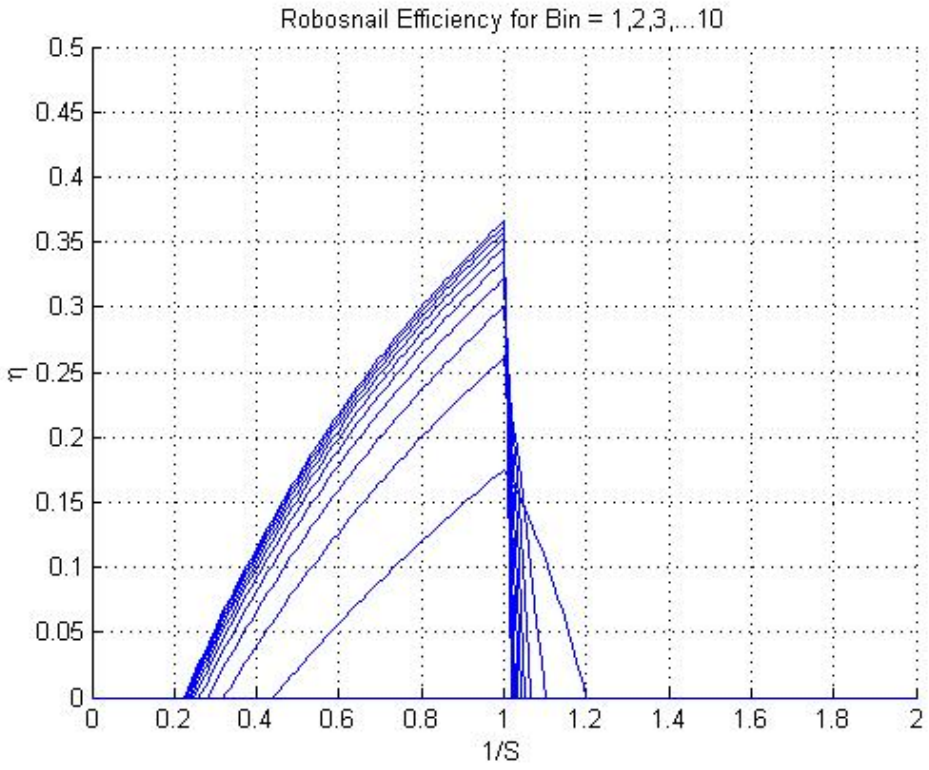

Figure 4-2: Tractoring efficiency for Robosnail 2, N = 6, varying the shear factor $f_s = \frac{\tau_i}{\tau_y}$. Curves shown for Bin = 1, 2, 3, ... , 10. The bottom curve is for Bin = 1.

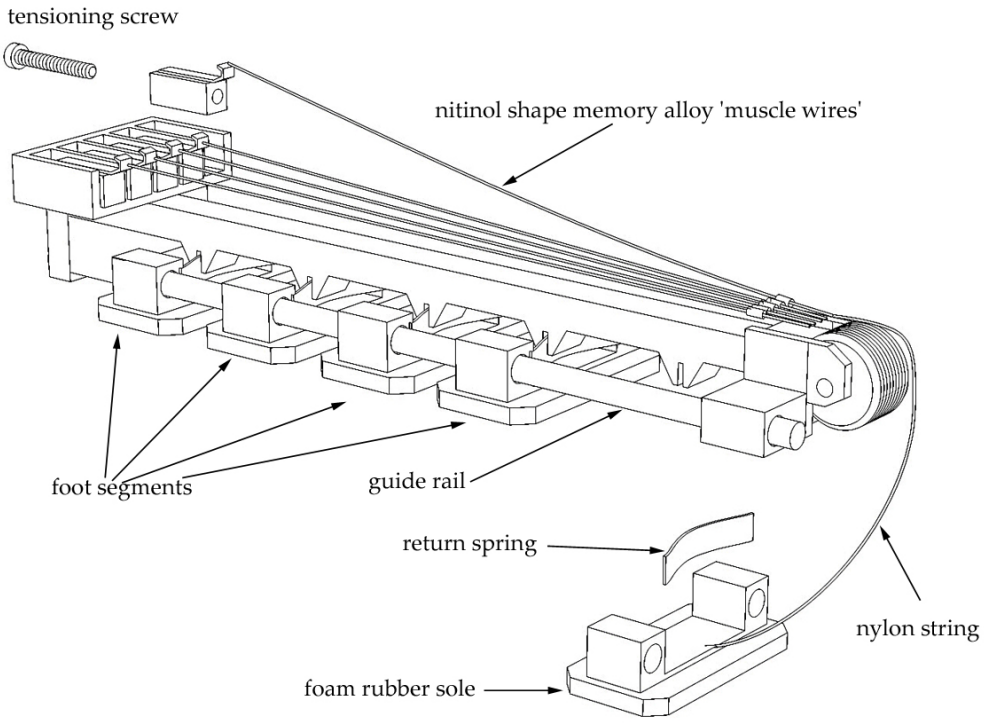

Figure 4-3: The first version of Robosnail 2 used shape-memory (Nitinol) wires to actuate the foot sections. This gave the advantage of compactness and minimized weight, but disadvantages were the slow and small movements of the segments (limited by the strain and cooling time required by the shape memory alloy) and the need for an umbilical cable.

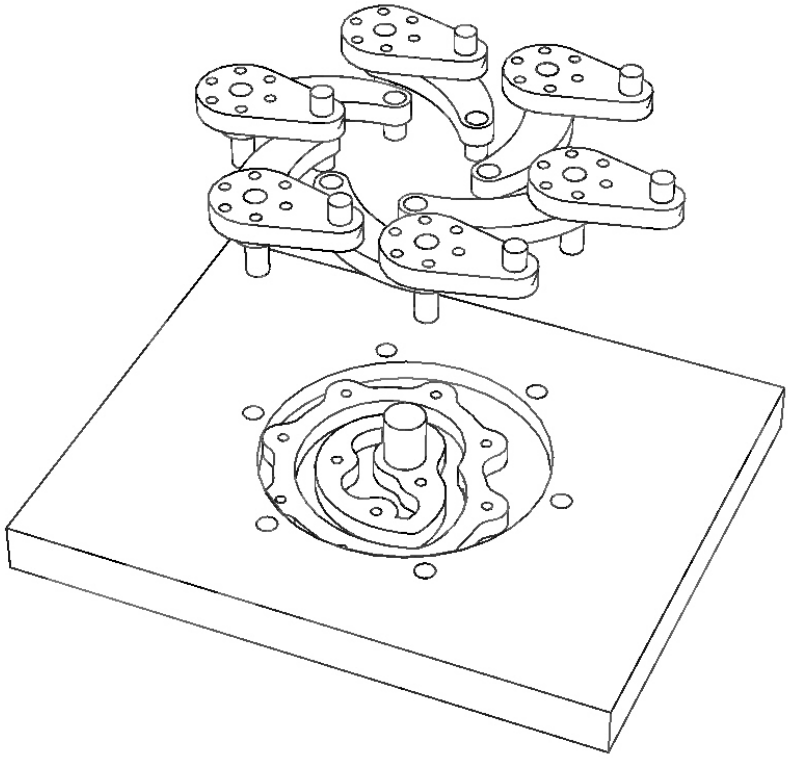

Figure 4-4: An exploded view of the internal transmission device of the second-generation Robosnail 2. The circular structure is the cam, surrounded by 6 followers. The followers each control one of the six foot segments in a linear motion.

The second finalized version of Robosnail (there were several trial versions that went uncompleted) is powered by a single motor, carries its own battery pack, and operates on an aqueous solution of Carbopol, a stronger yield-stress fluid with a faster restructuring time.

At the heart of Robosnail 2 is the newly developed transmission assembly which gives the separate foot pads their motion. The transmission consists of a slowly rotating disk/cam, which is powered by the motor via gearbox, a set of six arms which follow the track, and linkages between the arms and the foot pads. By guiding the positions of the arm tips as it rotates, the track groove on the rotating disk defines the motion of the foot pads.

We recall from the theory that for N pads, we want one of the pads (at any instant the wave pad) to be moving forward with a speed of $\hat{V}_w$, while the remaining pads move backwards at $\hat{V}_i$. The track shape to fit these requirements is one composed of two linear spirals, one steadily increasing radius over $(N-1)/N$ of the circle, and the other spiral connecting the ends of the long spiral over $1/N$ of the circle. The foot pads of Robosnail 2 are each mounted on a rigid linear slide, so they slide forward and backwards with minimal sideways deviation.

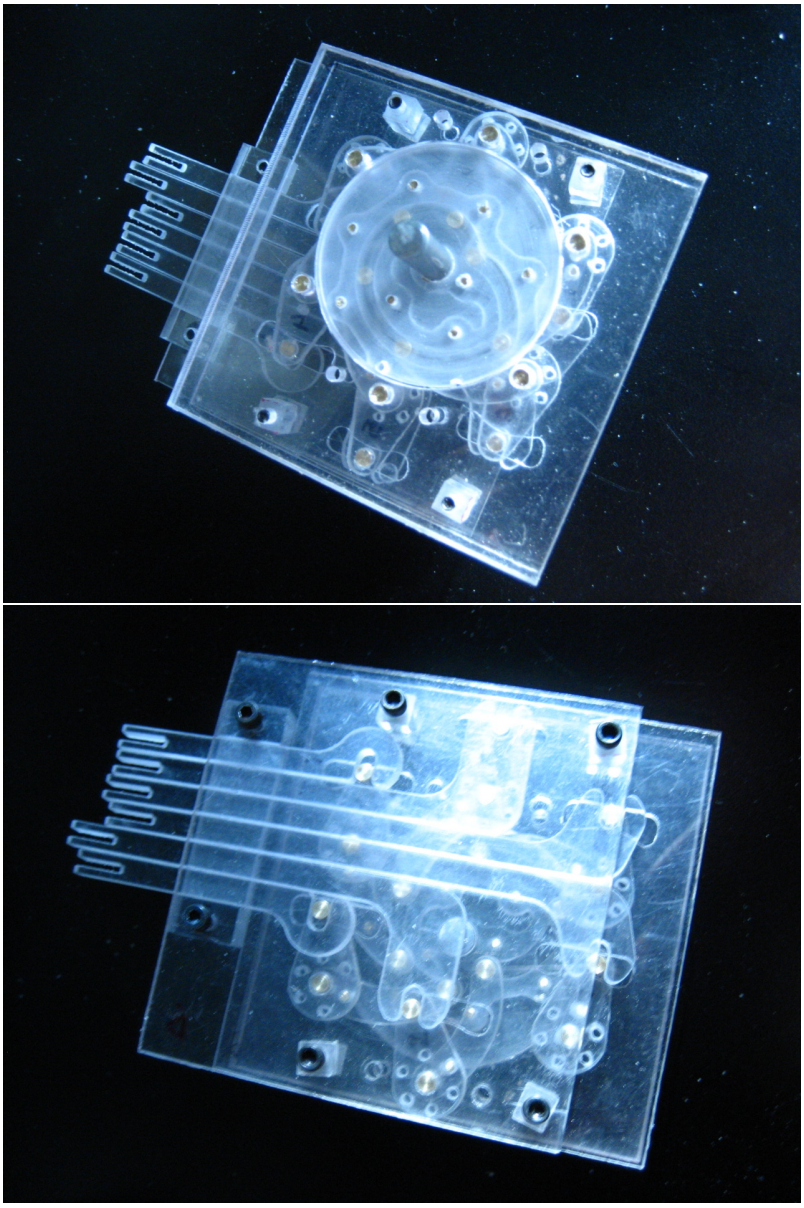

Figure 4-5: Top and bottom views of the cam device.

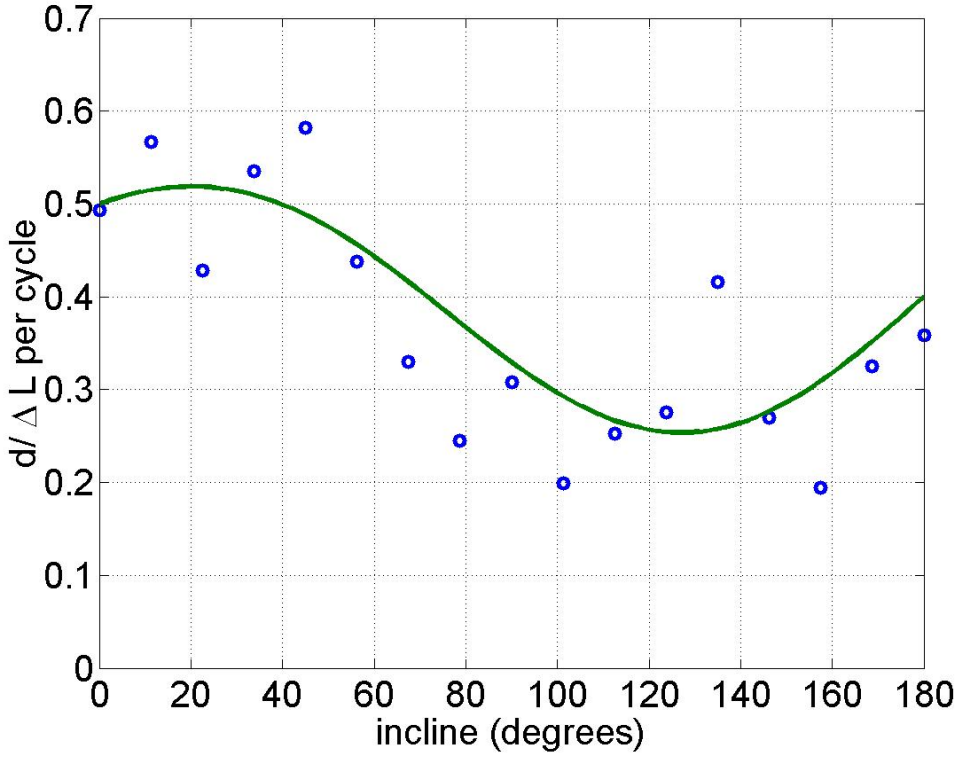

Figure 4-6: Displacement per cycle of Robosnail 2a, on Laponite solution 7.5 percent by weight. The snail functioned the best at 0 incline, where gravity was not pulling the snail against the direction of motion or away from the substrate. The worst performance occurred at 90 degrees vertical incline, when the snail had the most force pulling against its intended motion.

4.4 Experiment

The snail was run on a thin layer of fluid on various inclines. The fluid was first spread onto the surface in a layer that was more or less constant in thickness, then the snail was manually adhered to the surface. The first snail was tested with a solution of Laponite, an aqueous suspension of synthetic clay. The second generation, motor-powered model was tested solutions of Carbopol, a proprietary chemical of the Lubrizol corporation. The Carbopol has a much higher yield stress and so was able to support the bulkier snail.

4.5 Results and Discussion

As we expected, the snail operated better upright on a horizontally oriented plane than traveling up vertically or horizontally inverted. The worst results came from trying to move up a vertically inclined plane, with gravity pulling on the full weight of the snail. While inverted motion was not hindered by gravity in the direction of motion, the problem was that gravity caused the snail to delaminate and peel away from the surface. The first test, with the muscle wire snail operating on laponite, displayed the most forward motion at zero degrees (horizontal motion) , and the least motion at around 90 degrees (vertical motion).

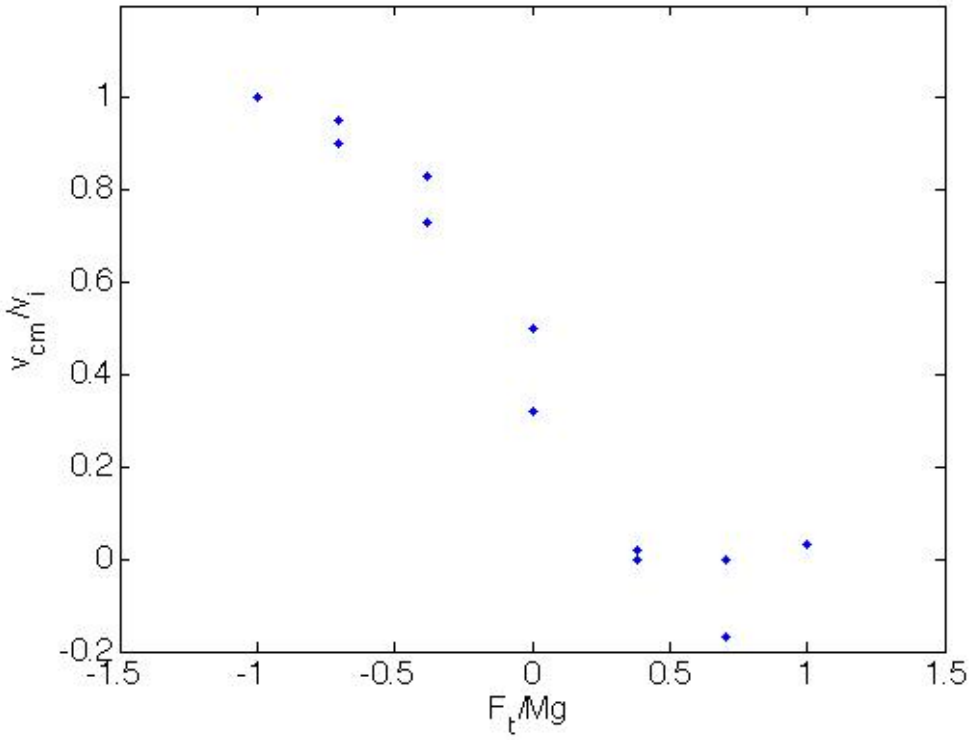

Figure 4-7: Robosnail 2 tractoring force vs. normalized tractoring velocity

Chapter 5

Three-Link Swimmer

5.1 Introduction

The Three-link swimmer was inspired by E.M. Purcell in his talk "Life at Low Reynolds Number" :

> There is a very funny thing about motion at low Reynolds number, which is the following. ...if (an) animal tries to swim by a reciprocal motion, it can't go anywhere. Fast or slow, it exactly retraces its trajectory and it's back where it started. ... The moral of this is that the scallop at low Reynolds number is no good. ...The simplest animal that can swim that way is an animal with two hinges. I don't know whether one exists ..."

In his talk, Purcell describes the realm of the low Reynolds number, where the effects of viscosity totally dominate, and momentum effects are negligible. Almost all swimming and flying organisms and devices known to man operate at high Reynolds number, where propulsive forces are generated by momentum. Because of this paradigm shift, many of the locomotion methods that are effective at low-Re are counterintuitive, and many high-Re locomotion methods become useless at low-Re.

Figure 5-1 illustrates the motion of the swimmer described by Purcell. During one cycle of motion, the swimmer executes four similar strokes. Because each of the fins flaps independently and out-of-synch with the other flap, the motion is not reciprocal.

5.2 Theory

At the limit of low Reynolds number (the Stokes limit), the Navier-Stokes equations reduce to the Stokes equations, which are time-independent [6, 1]. Because of this reversibility at the Stokes limit, reciprocal motions generate no net displacements.

A two-link swimmer such a simplified scallop, for example, is only capable of opening and closing. Whatever net motion experienced by the scallop in its opening stroke would be cancelled exactly during the closing stroke. Likewise, the rightward tail swing of a fishlike swimmer would cancel the effect of a leftward swing of its tail. Flapping wings, one of the most efficient methods of high-Re propulsion, becomes useless in the Stokes limit. Because of this property of reversibility, three links would be the minimum number of oscillating links required to compose a successful swimmer. (For non-reciprocating joints, two can suffice: as in the helical flagella swimmers, constant forward rotation in one direction comprises

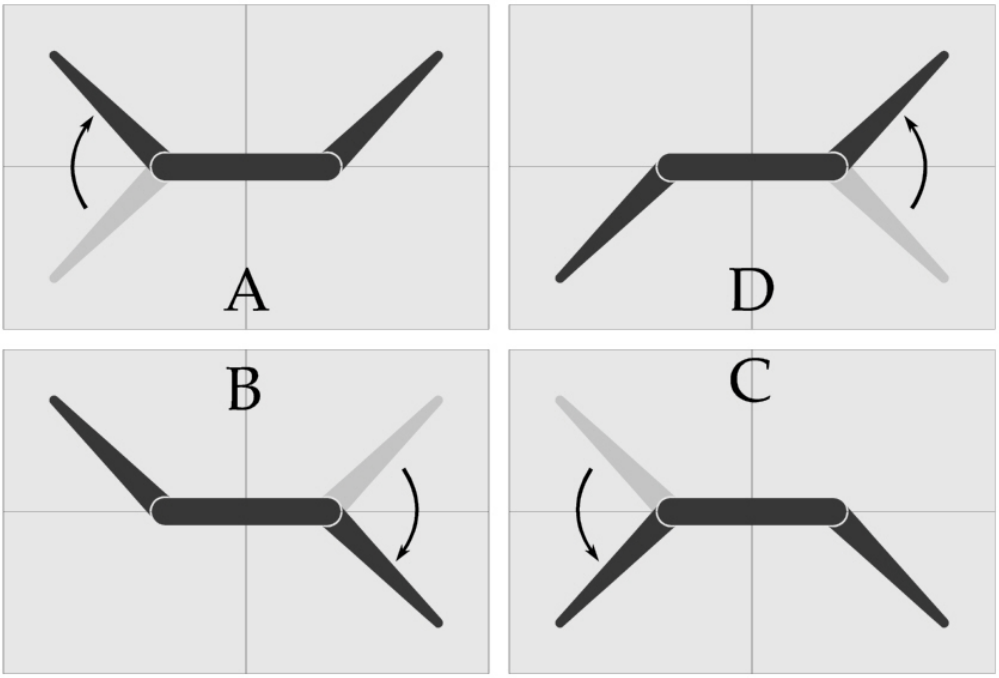

Figure 5-1: Motion sequence of three-link swimmer

non-reciprocal motion. Bacteria and sperm are two such helical flagella swimmers that exist in nature.).

5.2.1 Physics

The symmetry of the theoretical swimmer and its stroke pattern, and the reciprocal motion greatly simplify the analysis of the swimmer. In fact, one needs only analyze a single stroke to understand the entire motion of the swimmer, and can conclude that the swimmer must move in a straight line (Figure 5-2). This simplification is a result of two symmetries of the motion cycle: the flap of one fin is identical to the time-reverse flap of the second fin, while mirroring these two motions results in the third and fourth steps in the cycle.

There is also the question of the effect of increasing the size of the flapping fins in relation to the body. When normalized to the full body length, the fins are limited to being either zero length (an immobile body) or half the body length (no body, just fins, resulting in a two-link swimmer or scallop). As either of these cases results in zero displacement, there must be some optimal arm length a that maximizes the speed of the swimmer. Likewise, the angle of the stroke can also be optimized. It was found by Tam that the best stroke (for the planar swimmer composed of filaments) involves constant variation of both joints rather than discrete motion of one after the other, and that there existed separate optimizations for either maximizing the energy efficiency, or the displacement per cycle.

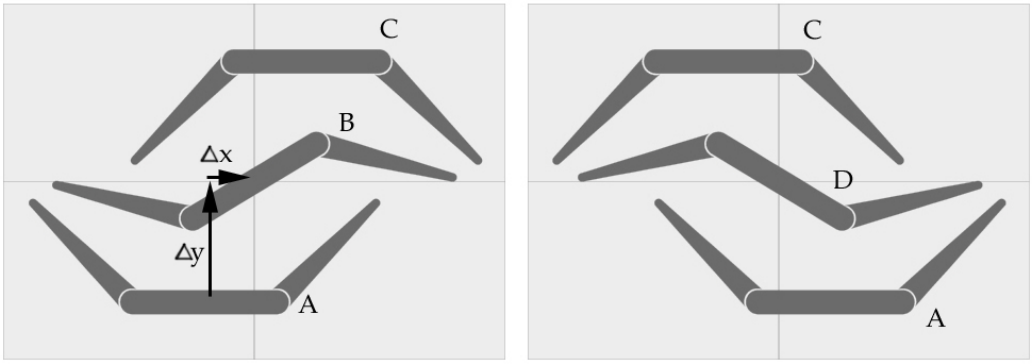

Figure 5-2: Hypothetical motion of the three link swimmer. The swimmer starts at "A", and flaps its right-side fin downward, moving the swimmer some x and y displacement δx, δy. From reversibility, this is the same as the reverse motion from B to C, and the sequence from C back to A is the same as the time-reverse mirror image from A to C. Thus we only need to know the motion from A to B to understand the full cycle.

5.3 Mechanical Design

The three-link swimmer was built to have three panel-like linkages, as opposed to long, narrow linkages as described in Purcell's talk and the literature. This was a practical compromise as the difficulties of placing the driving mechanism and power source in a narrow linkage would increase to the point of impracticality for a device that was to be small enough to operate at low Reynolds number.

The swimmer is powered by a clock spring, which led to a simpler design, and added the benefit of making the actuation mechanism smaller and less negatively buoyant compared to a motor-battery-gearbox assembly.

The spring generated a rotary motion, which would have to be translated to the reciprocal flapping of both end links (fins). To effect this flapping of the end links, we mounted the spring on its inner end and attached the free end to a rotating ring. The outer edge of the ring was shaped to have sloped sections in contact with part of the moving links/fins. As the ring rotated, the sloped edge would flip the fins to the left and right, causing the flapping motion. An important feature as discussed earlier was for the movement of one fin not to be simultaneous with the motion of the other fin. This is solved by placing the rotating axis of the ring to be offset from the imaginary line connecting the contact points of the fin.

All of the parts, with the exception of the spring and some small fasteners, were machined from polycarbonate and delrin plastics to keep the buoyancy to be as close as possible to neutral with respect to glycerol and silicone oil, which would be the intended working fluid. A small foam float was added to keep the device from sinking.

5.4 Experiment

As the only requirement for the fluid was for it to be Newtonian and of a significant viscosity, there were several choices for operating fluid. For practical reasons, we chose silicone oil, opposed to water soluble fluids, which would eventually corrode the steel clock-spring. The

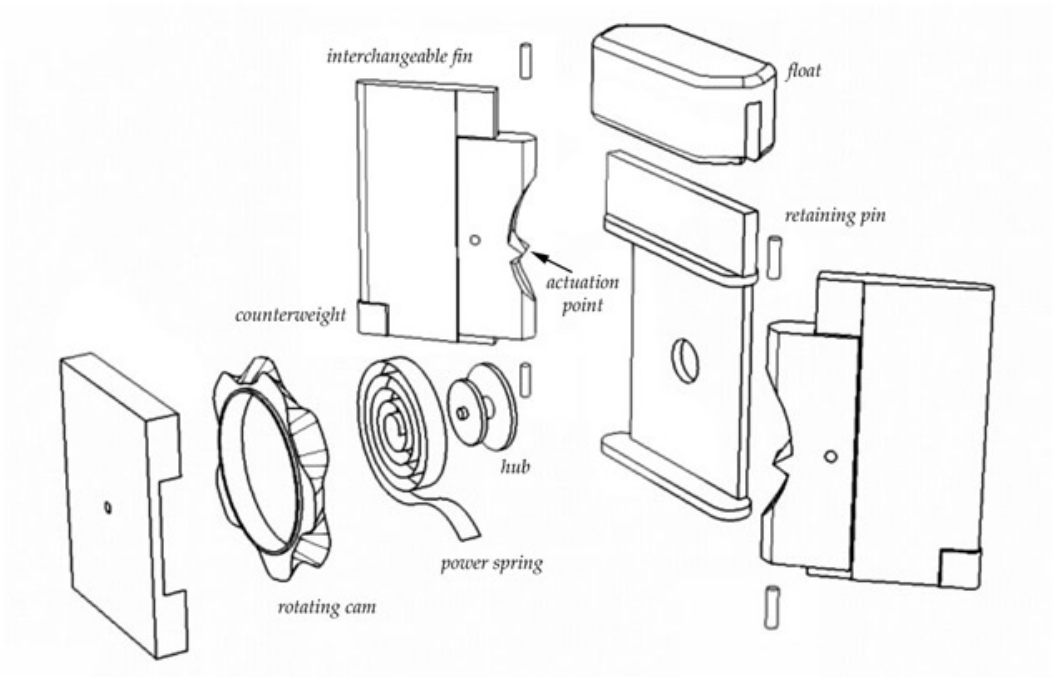

Figure 5-3: Exploded view of three-link swimmer

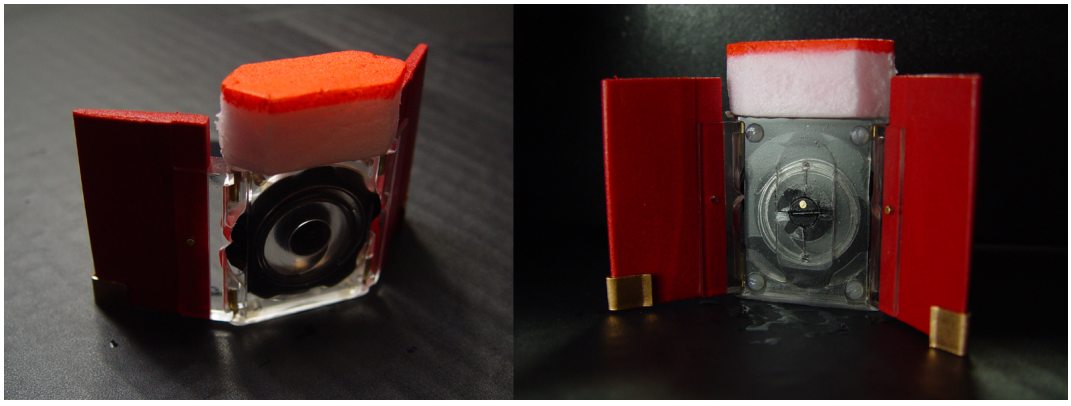

Figure 5-4: Exploded view of three-link swimmer

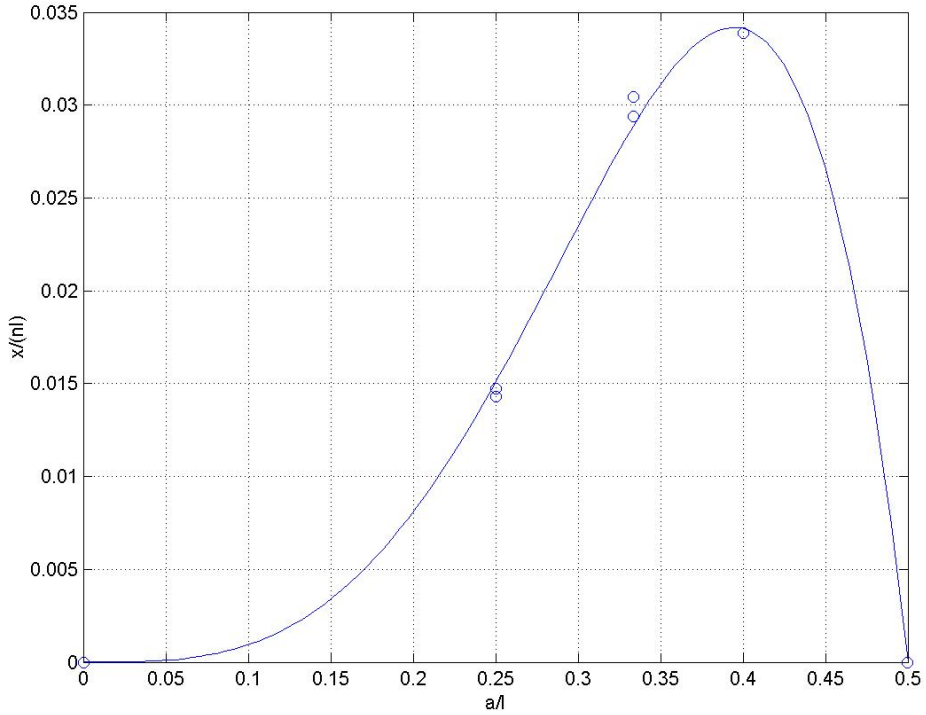

Figure 5-5: Distance traveled for the three-link swimmer, normalized to total unfolded body length, as a function of the fin/arm lengths. The data points at far left and far right (zero body length, vs. symmetrical two-link swimmer) were automatically set to zero because the theory predicts no motion. (The curve shown is a best-fit polynomial and not directly related to the theory.)

mechanical swimmer was operated with clear fluid to first test that there was positive travel. Later we put neutrally buoyant tracer particles and dye into the fluid to trace the fluid motion.

Another test would be to increase or decrease the arm lengths in relation to the body length and to experimentally find an optimal length to maximize the displacement per cycle.

5.5 Results and Discussion

First, the mechanical three-link swimmer successfully propelled itself through a high viscosity Newtonian fluid at a rate of several percentages of the body length per cycle. The displacement per cycle was shown to vary when the length of the arms were changed. Two arm-lengths besides 1:1 were tried and the displacements were normalized to the total swimmer length.

The experimental results seem to suggest an optimum arm size around b = 0.4, resulting in the maximum measured swimmer velocity near 0.034 body lengths per cycle. The flow around the three-link swimmer was fully 3D, and unlike the Becker swimmer, could not be analyzed with the theory of thin bodies. However, the real swimmer experiment provided us with qualitative information on the fluid dynamics of its swimming action. Like Becker, D.

Tam conducted extensive numerical studies in the search for an optimized swimming stroke and swimmer shape of a 3-link swimmer (Tam extends the analysis to compare optimal n-link swimmers and swimmers with a body). As the findings of Tam and Becker suggests, the optimized fin length is roughly equal to the body length, which was also the case for our prototype swimmer.

Neutrally buoyant tracer particles (kalliroscope rheoscopic fluid in some tests and small plastic beads in other runs) were planted in the fluid to trace the fluid motion as the swimmer propelled itself past. This low-tech flow visualization method allowed us to understand better the fluid dynamics of the swimmer.

Like any self - propelling body, the swimmer generates a thrust wake, pushing fluid backwards as it moves forward. There is however a large region of fluid being pulled along with the swimmer, as the no-slip condition is significant at the extremely low Reynolds number. Lastly because the fluid is incompressible, the fluid is pulled in from the sides to make up for the fluid moving to the fore and aft of the swimmer. Even after five cycles, these flow characteristics are clearly visible in the tracer lines.

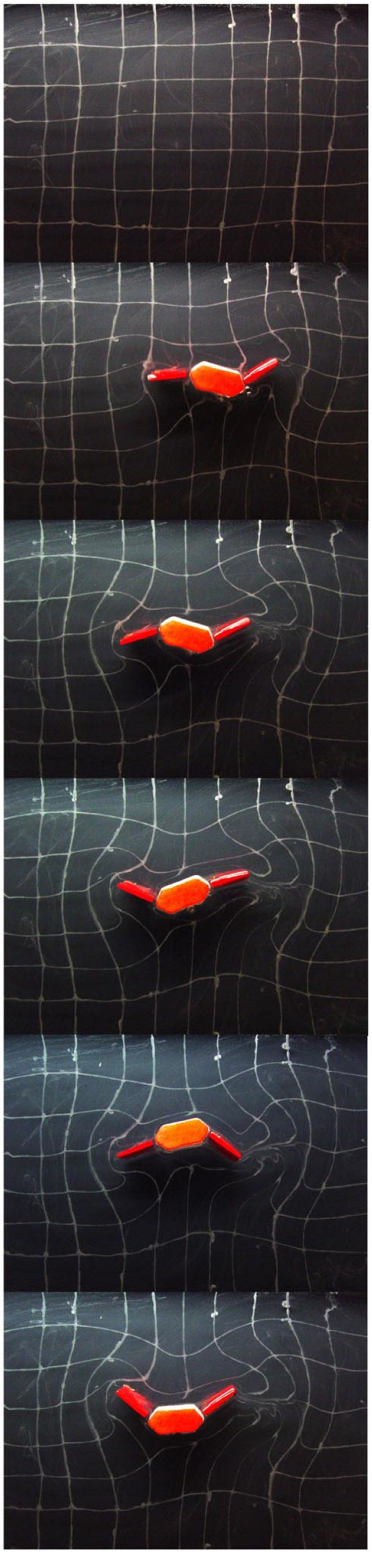

Figure 5-6: The three-link swimming next to fluid tracers. As the swimmer moves, it drags a portion of the fluid along with itself in the direction of motion, according to the no-slip condition, while simultaneously sending fluid backward in order to propel itself forward. As a result of fluid being forced forward and backward, the fluid is pulled in from either side of the swimmer, contracting lengthwise gridlines.

Chapter 6

Applications of Robosnail-type devices

6.1 General Applications

Robosnail 1 and Robosnail 2 - type robots can find find use in a variety of applications which require locomotion or the application of force, as long as high speeds are not essential. At low Reynolds numbers, i.e. high viscosity or small size, a robosnail-1 type robot would be effective in moving itself or other objects as long as there is a thin layer of fluid.

6.2 Downhole locomotion

In the oil drilling industry, it can be difficult to send various tools into the drilled holes, which are filled with mud. Mud will often limit traction, creating a lubrication layer that allows conventional gripping surfaces to slip on the substrate.

6.3 Rigless tool Deployment

In addition to sending powered tools and logging equipment into downholes, another application would be to use a stationary device to push tools into the downhole. Current technologies involve gripping tools with solid grippers, which risks damaging the surface of the tools from the stress concentrations at the gripping point.

Chapter 7

Conclusion

We have introduced three different types of locomotion, through viscous newtonian and non-newtonian fluids. Research on robosnail 1 has shown that peristaltic waves of a membrane can generate significant propulsive forces when lubricated with a newtonian fluid and brought close to a solid substrate. The theory and numerical simulations reveal the various characteristic forces and velocities that can be attained by changing the waving profile, and experimental results confirm the results for the basic, sinusoidal wave shape. The numerical simulations also showed the relative effect of leakage flows when the width of the snail was finite.

Robosnail 2 exploited the non-newtonian properties of aqueous suspensions of carbopol and laponite, shear-thinning fluids, to move in a way analogous to true snails which use shear-thinning mucus to climb walls and ceilings. Successful tests of wall climbing proves that snail like locomotion is indeed achievable for the mechanical device, using a synthetic mucus.

The three-link swimmer was shown to propel itself successfully as Purcell predicted. It was found that the swimming velocity was greatest when the fins were the same length as the body, this being the expectation as much smaller or much larger fins would be closer to the limiting cases where displacement is known to be zero.

7.1 Future work

The three-link swimmer was built as a proof-of-concept. While it functioned as we expected, it did not consist of a geometry as mathematically simple as the forms studied by Becker and Tam. The shape consisting of flattened panels was adopted as a matter of practicality. Future generations of the three-link swimmer should incorporate thin filamentous sections; we would expect the experimental results to closely match the theoretical results of Becker and Tam. In addition to three-link swimmer, Tam wrote numerical simulations of n-link swimmers, and found optimal swimming patterns for such multi-link devices. Experimental verification of these as well as other swimming methods would be important in the quest to build better low-Re devices.

Furthermore, the Tam swimmer varied from the prototype three-link swimmer in that not only was the optimal geometry studied, but the stroke cycle. It was found that the stroke pattern could be further optimized by incorporating overlapping strokes between the two fins; in other words, one fin would still be moving when the second fin begins to flap.

This research was done with the intention to determine the feasibility of these new types

of locomotion. While each of the devices was capable of locomotion in the way described by the theory, they were rigid and could only move in a straight line. The next obvious step would be to add control and steering. In the case of the snail, the goal would also include taking full advantage of a snail's flexibility by incorporating flexibility. The snail-like devices shown here were limited also by the fact that they did not carry their own mucus supply, unlike real snails. Future generations should be completely self-contained in this respect. It was mentioned in chapter **??** that later versions of Robosnail 1 employing various wave profiles would be optimized for various situations. It would be useful to design and test prototype snails that used these non-sinusoidal wave profiles.

Bibliography

[1] S. Childress. *The Mechanics of Swimming and Flying*. Cambridge University Press, Cambridge, 1997.

[2] M. Denny. "The role of gastropod pedal mucus in locomotion". *Nature*, 285:160–161, 1980.

[3] M. Denny. "Mechanical properties of pedal mucus and their consequences for gastropod structure and performance". *American Zoology*, 24:23–36, 1984.

[4] M. Denny. "Invertebrate mucous secretions: functional alternatives to vertebrate paradigms". *Journal of Experimental Biology*, pages 337–366, 1989.

[5] H.W. Lissman. "The mechanism of locomotion in gastropod molluscs, I. Kinematics". *Journal of Experimental Biology*, 21:58, 1945.

[6] E.M. Purcell. "Life at Low Reynolds Number". *American Journal of Physics*, 45:3–11, 1977.

[7] G.I. Taylor. "Analysis of the swimming of microscopic organisms". *Proceedings of the Royal Society of London, Ser. A*, 209:447, 1951.

[8] F Vls. "Sur les ondes pediuses de Mollosques reptateurs". *C. R. Hebd. Seances Acad. Sci.*, 145:276, 1907.